Received by OSTI

JUL 0 1 1988

BMI/ONWI/C--87

TI88 012371

INFLUENCE OF IMPURITIES ON THE CREEP OF SALT FROM THE PALO DURO BASIN

Francis D. Hansen
Paul E. Senseny
Tom W. Pfeifle
Tim J. Vogt

of

RE/SPEC Inc.

Prepared for

Office of Nuclear Waste Isolation
Battelle Memorial Institute
505 King Avenue
Columbus, OH 43201

May 1987

DISCLAIMER

This report was prepared as an account of work sponsored by an agency of the United States Government. Neither the United States Government nor any agency thereof, nor any of their employees, makes any warranty, express or implied, or assumes any legal liability or responsibility for the accuracy, completeness, or usefulness of any information, apparatus, product, or process disclosed, or represents that its use would not infringe privately owned rights. Reference herein to any specific commercial product, process, or service by trade name, trademark, manufacturer, or otherwise does not necessarily constitute or imply its endorsement, recommendation, or favoring by the United States Government or any agency thereof. The views and opinions of authors expressed herein do not necessarily state or reflect those of the United States Government or any agency thereof.

The content of this report was effective as of December 1985. This report was prepared by RE/SPEC Inc. under Contract E512-10000 with Battelle Memorial Institute, Project Management Division, under Contract DE-AC02-83-CH10140 with the Department of Energy. The contract was administered by the Office of Nuclear Waste Isolation.

MASTER

DISTRIBUTION OF THIS DOCUMENT IS UNLIMITED

DISCLAIMER

This report was prepared as an account of work sponsored by an agency of the United States Government. Neither the United States Government nor any agency Thereof, nor any of their employees, makes any warranty, express or implied, or assumes any legal liability or responsibility for the accuracy, completeness, or usefulness of any information, apparatus, product, or process disclosed, or represents that its use would not infringe privately owned rights. Reference herein to any specific commercial product, process, or service by trade name, trademark, manufacturer, or otherwise does not necessarily constitute or imply its endorsement, recommendation, or favoring by the United States Government or any agency thereof. The views and opinions of authors expressed herein do not necessarily state or reflect those of the United States Government or any agency thereof.

DISCLAIMER

Portions of this document may be illegible in electronic image products. Images are produced from the best available original document.

ABSTRACT

Twelve triaxial compression creep tests were performed on salt specimens from the Woods-Holtzclaw well in the Palo Duro Basin to assess the influence of impurities on creep deformation. Four nominal impurity levels were initially selected for investigation: pure salt, salt containing 10 percent anhydrite, salt containing 10 percent mud, and salt containing 20 percent mud. Subsequent petrological measurements show these idealized categories do not exist. Composition of the samples was measured by methods of wet chemistry coupled with ethylene diaminetetraacetic acid (EDTA) digestion and point counting on full-size polished sections. Overall, the 12 specimens comprise 71.6 to 96.6 percent halite, 2.4 to 7.5 percent anhydrite, and 0.2 to 24.7 percent clay. Nine of the 12 specimens are similar to many other tested specimens from the Lower San Andres Unit 5. They range from 90 to 97 percent halite and average 94 percent with a standard deviation of 2 percent. The remaining 6 percent impurities are disseminated clay and anhydrite. The other three specimens from the Lower San Andres Unit 4 contain large amounts (average 20 percent) of uniformly distributed clays and average only 75 percent halite.

All samples were tested at a temperature of 75°C, a confining pressure of 15 MPa, and a stress difference of 15 MPa. Test duration was 3×10^6s (35 days). The strain versus time data are fitted to the exponential-time creep law which has three fitting parameters. The parameter values are individually correlated with the amounts of halite, anhydrite, and clay. Anhydrite content has the strongest influence on the creep response. Increase in anhydrite reduces the steady-state creep rate, as well as the related axial strain. A weaker correlation is found between halite content and the creep parameters. No correlation exists between the amount of clay and the creep response. Variability of test results is not readily explained by amount and type of impurities.

FOREWORD

The National Waste Terminal Storage (NWTS) Program was established in 1976 by the U.S. Department of Energy's (DOE) predecessor, the Energy Research and Development Administration. In September 1983, this Program became the Civilian Radioactive Waste Management (CRWM) Program. Its purpose is to develop technology and provide facilities for safe, environmentally acceptable, permanent disposal of high-level waste (HLW). HLW includes wastes from both commercial and defense sources, such as spent (used) fuel from nuclear power reactors, accumulations of wastes from production of nuclear weapons, and solidified wastes from fuel reprocessing.

The information in this report pertains to rock mechanics studies of the Salt Repository Project of the Office of Geologic Repositories in the CRWM Program.

TABLE OF CONTENTS

		Page
1.0	INTRODUCTION	1
	1.1 BACKGROUND	1
	1.2 APPROACH AND SCOPE	1
	1.3 REPORT ORGANIZATION	3
2.0	SPECIMENS AND PREPARATION	5
	2.1 CORE ACQUISITION AND DESCRIPTION	5
	2.2 SPECIMEN PREPARATION	5
	2.3 NOMINAL IMPURITY CONTENT	6
	2.4 JACKETING	6
	2.5 POST-TEST DISPOSITION	8
3.0	TESTING AND PROCEDURES	9
	3.1 LOAD FRAME	9
	3.2 INSTRUMENTATION	11
	3.3 CALIBRATION	11
	3.4 CONTROL	11
	3.5 TEST PROCEDURES	13
	3.6 PETROLOGICAL PROCEDURES	14
	3.6.1 Mineralogy	14
	3.6.2 Etch Pit Studies	15
4.0	RESULTS	17
	4.1 MECHANICAL RESULTS	17
	4.2 IMPURITIES	23
	4.3 MICROPROCESSES	27
5.0	ANALYSIS	37
6.0	CONCLUSIONS	43
7.0	REFERENCES	45

TABLE OF CONTENTS
(Continued)

		Page
APPENDIX A.	STRAIN VERSUS TIME DATA FOR WOODS-HOLTZCLAW SALT . .	47
APPENDIX B.	REFERENCE LETTER FOR X-RAY FLUORESCENCE	63
APPENDIX C.	MECHANICAL RESULTS VERSUS IMPURITY CONTENT	67

LIST OF TABLES

Page

2-1. Nominal Impurity Content of Specimens 7

3-1. Calibration Results 12

4-1. Exponential-Time Parameter Values 22

4-2. Impurity Content of Specimens 26

5-1. Correlation of Mechanical Results and Impurity Content . . . 38

LIST OF FIGURES

Page

3-1. Creep Machine Load Frame 10

4-1. Axial Strain Versus Time Curves for Palo Duro Salt 18

4-2. Axial Strain Versus Time Curves for Four Natural Salts . . . 19

4-3. Axial Strain Versus Time Curves for Avery Island Salt: Machine Verification Tests 21

4-4. Scalar Creep Law Parameters Plotted as a Function of the Test Duration 24

4-5. Substructure of WH2570-0/1, $\varepsilon_1 = 0.035$, T = 75°C, $\sigma_1 - \sigma_2 = 15$ MPa, $\sigma_2 = \sigma_3 = 15$ MPa 31

4-6. Substructure of WH2383-0/1, $\varepsilon_1 = 0.045$, T = 75°C, $\sigma_1 - \sigma_2 = 15$ MPa, $\sigma_2 = \sigma_3 = 15$ MPa 32

4-7. Substructure of WH2468-0/1, $\varepsilon_1 = 0.047$, T = 75°C, $\sigma_1 - \sigma_2 = 15$ MPa, $\sigma_2 = \sigma_3 = 15$ MPa 34

5-1. Halite Content Versus Steady-State Strain Rate 40

5-2. Anhydrite Content Versus Steady-State Strain Rate 42

1.0 INTRODUCTION

1.1 BACKGROUND

Strength and deformational characteristics of crystalline solids are often controlled by small variations in impurities. For example, small amounts of carbon are used with iron to strengthen steel and cast iron. In metallurgy, the percentage and type of alloying elements are controlled to produce a material with specific properties. If the mixtures of constituents are allowed to vary, the properties of the products would no doubt be variable. Natural variability is often encountered in rock mechanics, and laboratory experiments usually measure properties of highly heterogeneous crystalline solids.

Bedded rock salt is a typical example of a naturally variable crystalline material. Composition of rock salt from different areas or even from different depths in one borehole is often highly variable. General differences are easily visible. For example, salt core from the Palo Duro Basin varies in appearance from milky white to dark gray-brown. Differences in color and darkness result from impurities, such as clays and anhydrite. In the process of measuring the experimental behavior of such heterogeneous material, mechanical differences among salt samples tested identically are often attributed to sample-to-sample variability, i.e., impurity content.

The distribution of impurities is potentially important to the mechanical response of natural rock salt samples. However, no known quantitative techniques exist for describing distribution of impurities. Distribution can only be qualitatively considered in this work. The impurities did not form structural features such as through-going bedding planes and could be classified, as a first approximation, as uniformly distributed. This investigation evaluates the effects of visible and measurable impurities on the creep of Palo Duro salt.

1.2 APPROACH AND SCOPE

Twelve specimens were tested at identical stress and temperature to determine the influence of impurity content on creep deformation.

Specimens were selected from the Woods-Holtzclaw well representing four nominal impurity levels: pure salt, salt containing 10 percent anhydrite, salt containing 10 percent mud, and salt containing 20 percent mud. (Careful petrographic measurements subsequently showed that the nominal classifications are not sufficiently accurate.) A triaxial compression creep test was performed on each of the twelve specimens. The conditions were identical for each test: temperature was 75°C, confining pressure was 15 megapascals (MPa), and stress difference was 15 MPa. Each test was run for 3×10^6s (~35 days). Previous tests performed on Palo Duro salt indicate that moderate strains (about 5 percent axial strain) would be obtained at these test conditions over this time period [Senseny et al., 1985; 1986]. Therefore, if the impurities caused large differences in creep deformation, adequate accuracy and resolution would be available for smaller strains and adequate test machine range would be available for larger strains. The stress and temperature selected for these tests are representative of those expected in the room region of a nuclear waste repository. The test duration was selected so that the tests could be performed within the allotted time for this study. The duration was not great enough so that the data can be used to evaluate parameters in the exponential-time constitutive model. However, the fits to individual tests, which were all of identical duration, provide comparable parameters that can be used for comparison purposes. The fit of an exponential-time function to the individual strain-time curves calculates a steady-state rate, a value for asymptotic transient strain and a rate parameter for each test. These parameters are used for evaluation of the effects of impurities.

The axial strain versus time data from each test were fitted to the exponential-time creep law to provide a quantitative description of the creep deformation. The values of the fitting parameters are correlated to the measured type and amount of minerals in the sample, i.e., halite, anhydrite, and clay. The hypothesis underlying this study is that visible impurities influence the creep of salt to a measurable extent and in a consistent way. The results show that only anhydrite content has a moderately strong influence on the creep behavior under these test conditions.

1.3 REPORT ORGANIZATION

The remainder of the report is divided into five chapters and three appendixes. Chapter 2 describes the specimens used in this study, and Chapter 3 describes the test machines used and gives the test procedures. Creep test data, chemistry, petrology, and microstructural results are given in Chapter 4, and Chapter 5 analyzes the data. Chapter 6 gives the conclusions of this study and is followed by a list of cited references. Appendix A gives the axial and lateral strain-versus-time curves for each of the 12 tests. Appendix B is a letter from Pacific Northwest Laboratory [Laul, 1984] concerning X-ray fluorescence data. Appendix C contains plots of the creep parameters versus impurity content.

Missing Page
from
Original Document

2.0 SPECIMENS AND PREPARATION

2.1 CORE ACQUISITION AND DESCRIPTION

The specimens for this experiment were prepared from 100-mm- (4-in-) diameter core from the Woods-Holtzclaw well near Amarillo, Texas, in the Palo Duro Basin. Twelve specimens were selected by Office of Nuclear Waste Isolation (ONWI) personnel in conjunction with personnel from the Texas Bureau of Economic Geology and Stone & Webster Engineering Corporation. The cores were selected on the basis of nominal impurity content (see Section 2.3).

2.2 SPECIMEN PREPARATION

The specimens were right circular cylinders and had nominal dimensions of 100-mm (4-in) diameters and 200-mm (8-in) lengths, i.e., length-to-diameter ratios, L:D ≈ 2.

To obtain specimens with these dimensions, the cores were cut to approximate length using a cutoff saw having a diamond blade and Almag oil as the cutting fluid. The specimen ends were finished by mounting the sawed core in a vertical milling machine and cutting them flat and parallel within 0.02 mm (0.0008 in) using carbide tooling.

After each specimen was finished, it was assigned an identification number, logged into the RE/SPEC computerized inventory, and sealed in a plastic bag for storage. A typical identification number is

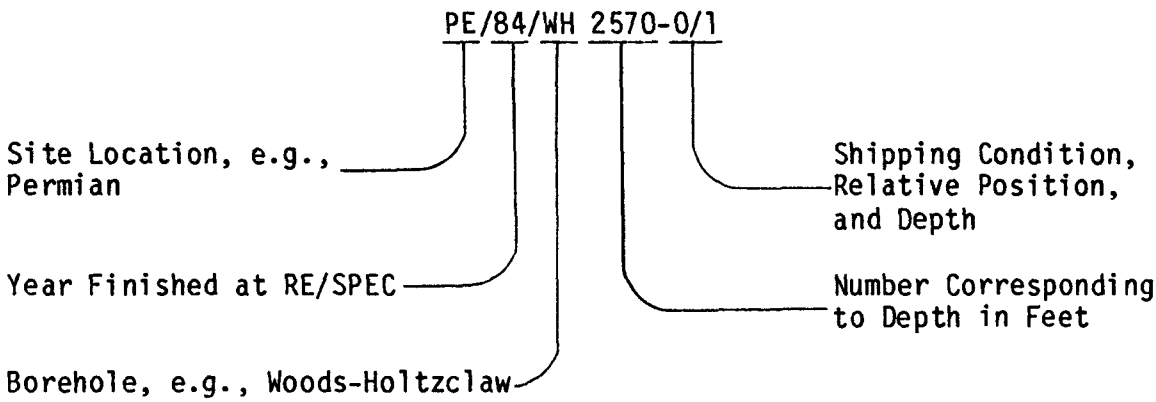

2.3 NOMINAL IMPURITY CONTENT

This experimental work was performed to evaluate the effects of impurities on the creep behavior of salt from the Palo Duro Basin. The samples were initially selected and grouped into nominal impurity level categories. Table 2-1 lists the 12 specimens, their depth, and their nominal impurity content, as determined visually at the time of selection. Actual impurity content is quite different from the nominal values (see Section 4.2). The specimen depths correspond to Unit 4 and Unit 5 of the Lower San Andres Formation. Initial statistical studies of the mechanical results using nominal impurity contents showed that the variability between impurity levels is insignificant when compared to the variability among specimens of the same nominal impurity level. If actual impurity content levels are used, the statistical analysis leads to some significant impurity effects.

The precise mineralogy of each sample is presented in Section 4.2. The petrology of this suite of samples ranges from 75 to 95 percent halite, 1 to 15 percent anhydrite, and 0 to 18 percent clay and is only generally related to the visually estimated impurity content. For purposes of impurity determinations, the initial nominal categories are not substantiated and are not considered within the remainder of this report.

2.4 JACKETING

The specimens were jacketed to prevent the confining pressure fluid from entering the pore space during the tests. Initially, the specimens were inspected for any pits that may have resulted from coring. These pits were filled with a silicone sealant to prevent jacket intrusion under pressure. The specimens were then placed between two cylindrical steel platens with a molybdenum disulfide dry lubricant placed in the specimen-to-steel interfaces. A length of 1.6-mm- (0.06-in-) thick Viton tubing was then slipped over the assemblies and sealed to each platen with stainless steel lock wires. The Viton jacket will withstand temperatures of 200°C.

Table 2-1. Nominal Impurity Content of Specimens

Specimen ID	Depth (feet)	Unit	Nominal Impurity Content
PE/84/WH 2450-0/1	2,449.8 - 2,450.7	5	Pure Salt
PE/84/WH 2453-0/1	2,452.7 - 2,453.5	5	Pure Salt
PE/84/WH 2509-0/1	2,508.9 - 2,509.7	5	Pure Salt
PE/84/WH 2383-0/1	2,382.8 - 2,383.6	5	10% Anhydrite
PE/84/WH 2448-0/1	2,447.2 - 2,448.0	5	10% Anhydrite
PE/84/WH 2468-0/1	2,467.5 - 2,468.3	5	10% Anhydrite
PE/84/WH 2376-0/1	2,375.5 - 2,376.3	5	10% Mud
PE/84/WH 2443-0/1	2,442.9 - 2,443.8	5	10% Mud
PE/84/WH 2464-0/1	2,463.8 - 2,464.6	5	10% Mud
PE/84/WH 2570-0/1	2,570.0 - 2,570.9	4	20% Mud
PE/84/WH 2578-0/1	2,577.2 - 2,578.1	4	20% Mud
PE/84/WH 2655-0/1	2,654.2 - 2,655.0	4	20% Mud

2.5 POST-TEST DISPOSITION

After each specimen was tested, it was sealed in a plastic bag with an identification tag. Later, the specimen was sectioned for analyses that included petrography, chemistry, and deformed microstructure. Tested specimens and unused core will be returned to the Texas Bureau of Economic Geology core facility. An inventory record of all core is kept in the RE/SPEC offices.

3.0 TESTING AND PROCEDURES

The triaxial compression creep tests were conducted using six of ten identical machines in the RE/SPEC laboratory. They are very similar to those designed by Dr. W. R. Wawersik of Sandia National Laboratories. Descriptions of these machines have been presented in a previous publication [Mellegard et al., 1983]. These machines have the distinctive capability of measuring volumetric changes during a triaxial compression test. The algorithm for reducing volumetric measurements to average lateral strain was developed in that report, and the derivation is not included here.

3.1 LOAD FRAME

Figure 3-1 presents a cross section of a typical load frame for creep testing with prominent components labeled for reference. The machines use a single-ended, triaxial pressure vessel that accommodates a 100-mm- (4-in-) diameter cylindrical specimen having a length-to-diameter ratio of L:D = 2. A hydraulic cylinder bolted to the base of the load frame drives the loading piston which applies axial compressive force to the specimen. Confining pressure is applied to the jacketed specimen by pressurizing the sealed vessel chamber with silicone oil. A dilatometer system maintains constant confining pressure and provides the volumetric measurement for making lateral strain calculations.

The testing machines can apply compressive axial loads up to 1.5 meganewtowns (MN) and confining pressures up to 70 megapascals (MPa). The heating system (including seals on the pressure vessel) can maintain specimen temperatures up to 200°C.

A control panel houses the accumulators, hydraulic pumps, pressure intensifiers, transducer signal conditioning, temperature controllers, and confining pressure controllers for two adjacent test frames. The panels contain digital meters that display the output of the transducers. The temperature controller gives a digital output of the temperature. Mechanical pressure gages mounted in the panel give readings of the nitrogen pressure in the accumulator and the oil pressure in the hydraulic cylinder.

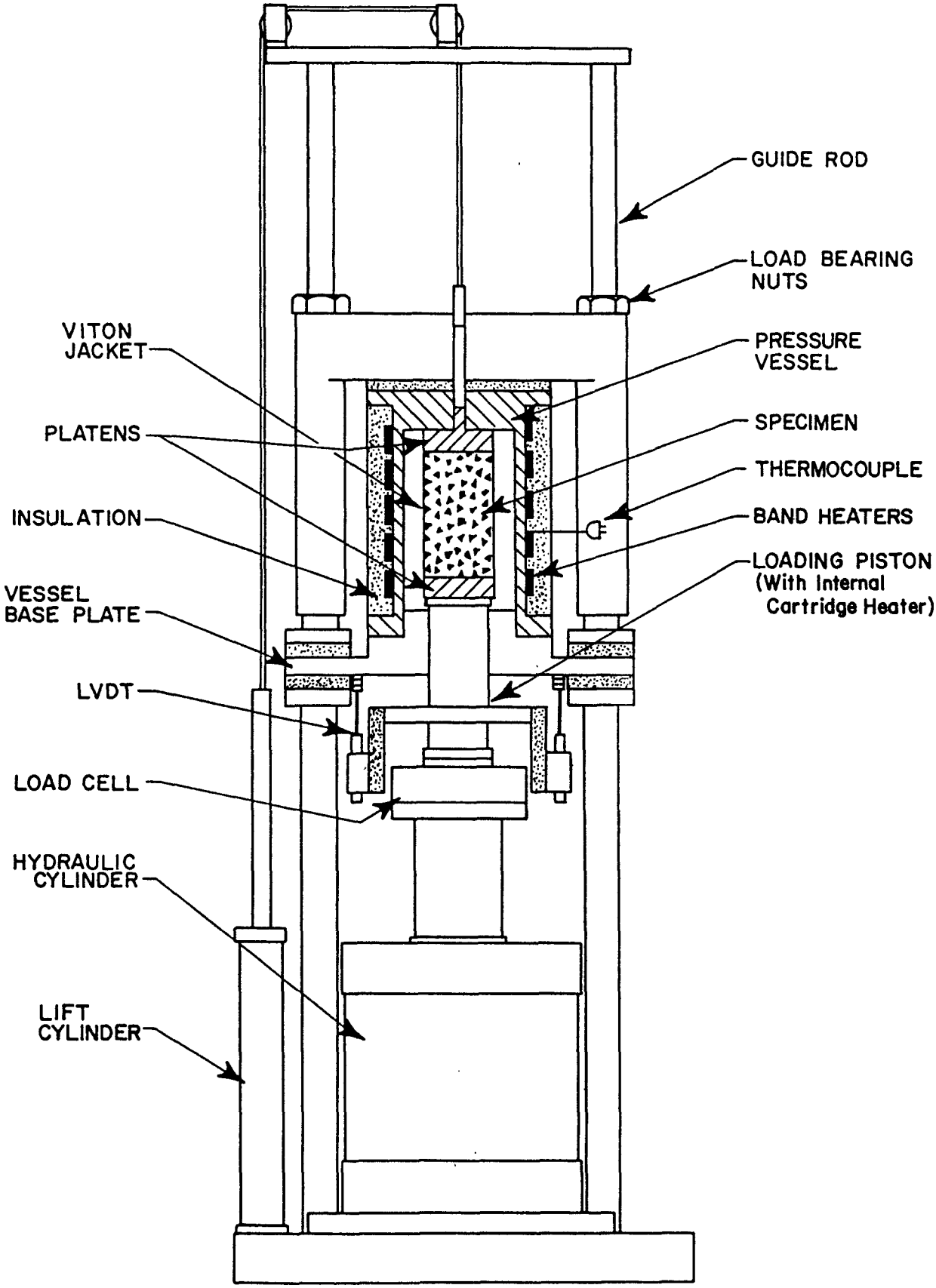

Figure 3-1. Creep Machine Load Frame [Mellegard et al., 1983]

3.2 INSTRUMENTATION

Axial force is measured by a load cell in the load column outside the pressure vessel, while confining pressure is measured by a pressure transducer in the line between the intensifier and the pressure vessel. Temperature is measured by a thermocouple in the wall of the pressure vessel. The relationship between specimen temperature and the temperature in the pressure vessel wall has been determined by calibration runs at several temperatures that span the operating range. Axial deformation in the specimen is measured by two linear variable displacement transducers (LVDTs) mounted outside the pressure vessel. They monitor displacement of the loading piston relative to the bottom of the pressure vessel, and during data reduction their output is corrected to account for test machine deformation. Lateral deformation is measured using a dilatometer. With this technique, lateral deformation is determined at fixed pressure by measuring the volume of oil that the intensifier withdraws from the pressure vessel, and then compensating for the axial deformation measured by the LVDTs. A rotary potentiometer is mounted on the intensifier shaft to provide a signal proportional to the volume of oil withdrawn from the pressure vessel.

3.3 CALIBRATION

The transducers used to collect data are calibrated using standards traceable to the National Bureau of Standards. Table 3-1 gives accuracy and resolution for the transducers. The value reported for accuracy includes both nonlinearity and repeatability. Resolution is based on a 14-bit analog-to-digital converter.

3.4 CONTROL

Temperature is controlled by a manual set-point controller that regulates power to both the band heaters on the vessel and the cartridge heater in the piston. The thermocouple in the pressure vessel wall supplies the feedback signal. The specimen temperature is maintained constant within 0.2°C (0.4°F). Confining pressure is regulated by

Table 3-1. Calibration Results

Measurement	Range	Accuracy	Resolution[a]
Axial Strain (Percent)	0-13.5	0.006	0.0007
Lateral Strain (Percent)	0-8.0	0.004[b]	0.002[b]
Axial Load (MN)	0-0.5	0.001	0.0002
Confining Pressure (MPa)	0-70.0	0.035	0.009
Temperature (°C)	25-200.0	1.0	0.02

(a) 14-bit analog-to-digital converter.
(b) Accuracy and resolution determined at zero axial strain.

entering the pressure transducer signal to a controller containing two manual set points. These set points are adjusted to maintain the confining pressure constant within 20 kilopascals (kPa). When a set point is reached, the controller signals the intensifier to advance or retreat, depending upon which set point has been reached. Axial load is controlled by a Digital Equipment Corporation (DEC) PDP-11/23 minicomputer. The computer determines the current cross-sectional area of the specimen from the outputs of the deformation transducers and then adjusts the load to maintain constant stress. The deadband on load under computer control is 0.6 kilonewtons (kN), and for 100-mm- (4-in-) diameter specimens, gives a deadband on axial stress of 75 kPa.

3.5 TEST PROCEDURES

The tests are initiated by the operator, but are controlled by a PDP-11/23 computer. First, a hydrostatic stress equal to the confining pressure is applied to the specimen, and the dilatometer servosystem is actuated to maintain constant pressure. The system is allowed to stabilize and the specimen is then heated to the desired temperature and allowed to stabilize for 12 hours. Next, the operator enters the specimen dimensions, the desired axial stress, and the confining pressure into the computer. The computer outputs the axial load required to obtain the axial stress, assuming no change in specimen diameter. The operator increases the axial load to this value within 30 seconds using the panel meter display as feedback, and then immediately gives control of the test to the computer. The computer, which has monitored specimen deformation under operator loading, immediately increases the load to give the desired stress. The computer monitors specimen deformation and the axial force every 30 seconds, if necessary, adjusting the force to maintain constant stress throughout the test. Axial force is adjusted using two solenoid valves that, when opened, either add nitrogen to the accumulator or vent nitrogen from it. The data channels are scanned at a selectable rate, typically every 15 seconds. Data are saved according to one of two criteria. First, if the specimen length changes by a prescribed amount since the last data were logged, data are logged again. If, however, the specimen length changes by less than the

prescribed amount over a time selected by the operator, data are logged at the end of this time period.

3.6 PETROLOGICAL PROCEDURES

3.6.1 Mineralogy

Mineralogy of the test specimens was measured three different ways (excluding the visual guesses): (1) X-ray fluorescence, (2) wet chemistry, and (3) optical microscopy.

X-ray fluorescence (XRF) was conducted by Pacific Northwest Laboratory [Laul, 1984] on the salt cores before they were finished and tested. XRF analyses were completed for the following elements: chlorine (Cl), calcium (Ca), titanium (Ti), iron (Fe), lead (Pb), bromine (Br), and strontium (Sr). Weight percentages of halite and anhydrite (see Table 4-2) are calculated by assuming all of the Cl is chemically bound in halite and all the Ca is bound in anhydrite. Calculations of halite and anhydrite percentages are straightforward; the weight of halite is 1.649 times the weight of the measured Cl, and the weight of anhydrite is 3.397 times the weight of Ca. These multipliers are calculated by dividing the atomic weight of the mineral by the atomic weight of the pertinent element. The amount of clay is assumed to be the difference between 100 percent and the total of halite and anhydrite. Estimates such as these contain variable but quantifiable errors. The error is assumed to be approximately equivalent to the natural variability within the sample. For example, the weight percentage of Cl as measured by XRF along the length of a sample is typically about 50 percent with a standard deviation of about 2 percent.

Wet chemistry analyses were completed for Ca, magnesium (Mg), sodium (Na), potassium (K), Sr, Cl, and sulfates (SO_4). The water insoluble residue is clay and anhydrite that did not dissolve in the aqueous digestion. Subsequent to the wet chemistry, an ethylene diaminetetraacetic acid (EDTA) procedure dissolves the residual anhydrite, leaving only clays. The halite percentage is readily determined by adding the weight percent of Na and Cl, even though the ratio of Na and Cl rarely exactly balanced stoichiometrically. Anhydrite is

not readily soluble in pure water but is somewhat soluble in the brine produced during the water digestion. Total anhydrite as calculated from the wet chemistry data is the sum of the Ca and SO_4 analysis plus the loss of weight from the aqueous residue to the EDTA residue. The assumption that all the Ca and SO_4 is in the mineral anhydrite is supported by a near balance stoichiometrically.

Petrographic mineral identification uses polished thick sections of the entire sample. The sections are made by first sawing the tested specimen in half along its axis and polishing one half. The polished half is epoxied to a glass slide (roughly 100 by 200 mm [4 by 8 in]) and cut to a thickness of about 3 mm (0.12 in). This full-size megasection is then polished and used for point counting. A Zeiss photomicroscope with capabilities of incident or transmitted light is used for observational work. Each section was counted 1,000 times by traversing the central three-fourths of the sample at grid intervals of 2.5 by 5 mm (0.10 by 0.20 in).

3.6.2 Etch Pit Studies

The substructures of each sample are studied using etch pit techniques. Cleaved chips are extracted from the central portion of the tested sample. These chips are immersed and vigorously agitated for five seconds in methanol saturated with $PbCl_2$. This etches the surface by preferential dissolution of dislocation sites. The etch process is stopped by rinsing in butanol. The etched chips are studied under reflected light using a Zeiss photomicroscope.

Missing Page
from
Original Document

4.0 RESULTS

4.1 MECHANICAL RESULTS

Only 11 of the 12 tests were successfully completed. In the unsuccessful test, the jacket leaked after about 0.35 x 10^6s (~4 days). Appendix A gives plots of axial and lateral strain as functions of time for individual tests. Figure 4-1 plots the axial strain-versus-time curves for all 12 tests. Each test sample is identified by its depth. The unsuccessful test is apparent; at the time of the jacket leak, the rate of deformation increased sharply. With the exception of the unsuccessful test, the strains at the end of the tests range from 0.02 to 0.085, a factor of more than four. This variability is roughly the same as measured on salts from different sites in the United States. In Figure 4-2 strain-time data for four different salts - Avery Island, Salina, Palo Duro Unit 4, and Palo Duro Unit 5 - are plotted for the same temperature, stress difference, and confining pressure used in the experiments to measure the effect of impurities (75°C [167°F], 15 MPa, and 15 MPa, respectively). At a time of 2 x 10^6s (~23 days), the strain magnitudes range from 0.025 to 0.095 (Figure 4-2). Note that the response of the Palo Duro Unit 4 and Unit 5 experiments in Figure 4-2 is within the central cluster of data on Figure 4-1. Also note in Figure 4-2 that the very clean Avery Island salt strains far more than any of the less pure salts. Overall variability of salt, such as shown in Figures 4-1 and 4-2, is routinely (but perhaps erroneously) attributed to impurity content.

The variability in Figure 4-1 is larger than observed for Avery Island salt specimens which average 99 percent halite and less than 1 percent anhydrite. When the six load frames used in this study were delivered to our laboratory, creep tests were performed on specimens of Avery Island salt to assure that test results from the new load frames were consistent with those obtained from the four load frames already in use. Triaxial compression creep tests were conducted at a temperature of 100°C (212°F), a confining pressure of 15 MPa, and a stress difference of 12.5 MPa. Later, two more tests were conducted on Avery Island salt under identical conditions; results are included here for

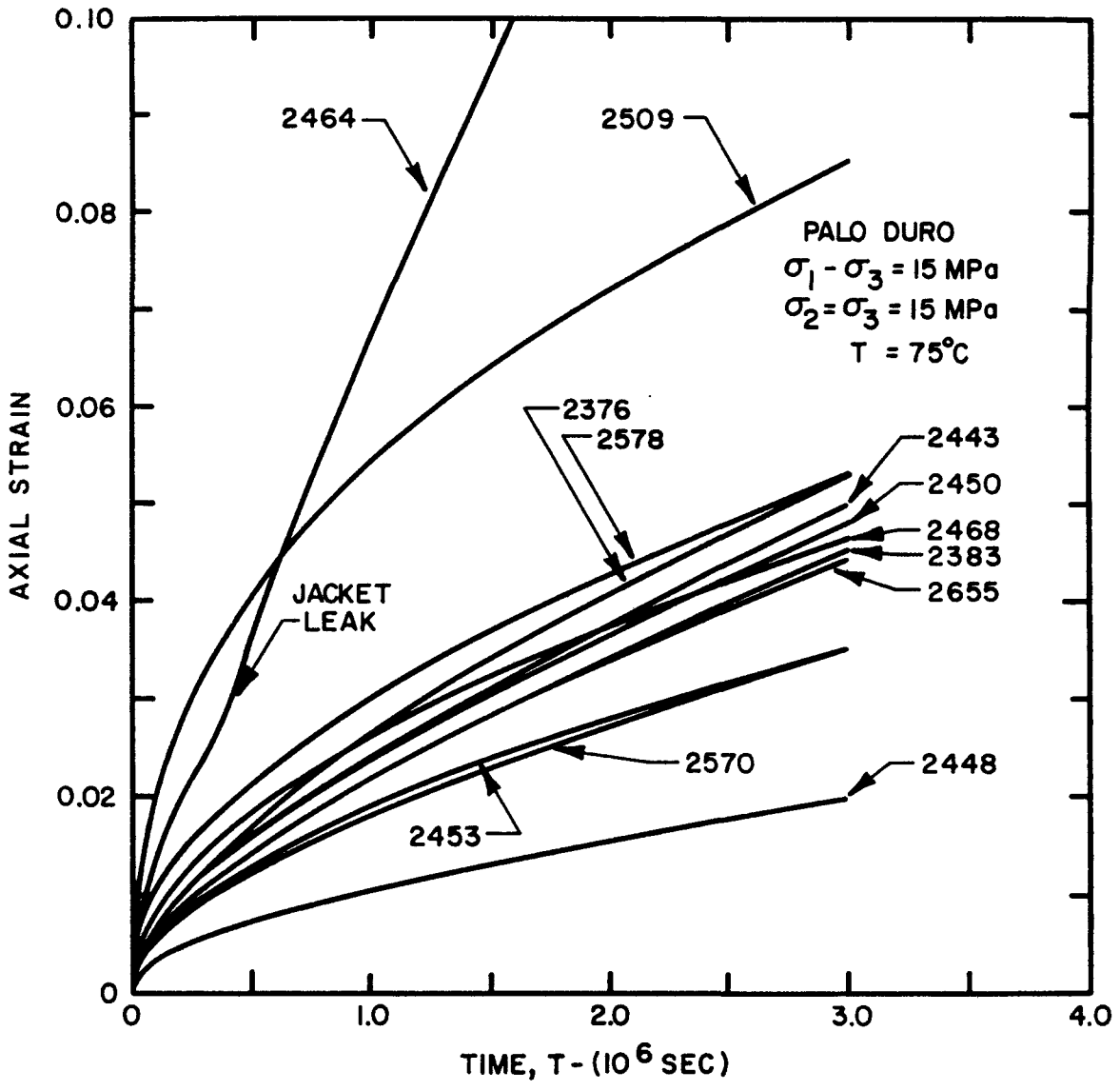

Figure 4-1. Axial Strain Versus Time Curves for Palo Duro Salt

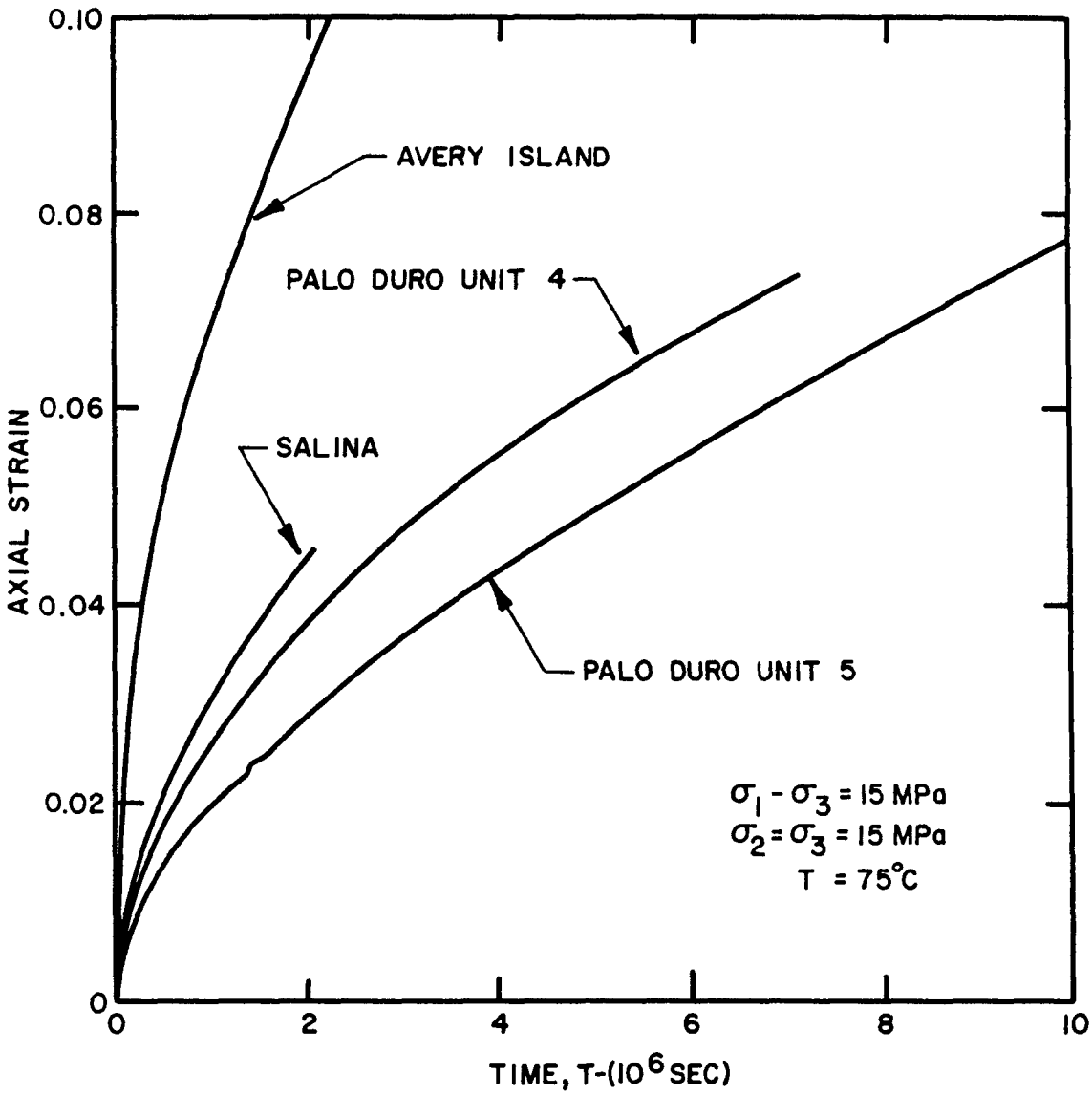

Figure 4-2. Axial Strain Versus Time Curves for Four Natural Salts

completeness. Figure 4-3 plots the axial strain-versus-time curves obtained from the six tests performed in the new load frames plus one subsequent test under identical conditions. Five of the curves are within a 10 percent grouping. Four of these five samples originated from Heater Site A on the 152-m (500-ft) level of the Avery Island mine. One came from Heater Site C located about 61 m (200 ft) from Site A on the same level. All five samples were prepared in the same batch in 1979. One of the curves that lies well above (about 30 percent) the cluster of five represents a sample (prepared in 1982) from a location in Avery Island called C', which is situated approximately 12 m (40 ft) from Heater Site C. Another study on Avery Island salt [Handin et al., 1984] also found that specimens from the C' location were weaker than those from the heater sites despite having essentially identical mineralogy. Finally, the experiment exhibiting by far the largest strain (about 50 percent more than the cluster of five) was run almost a year later than the original six tests. The sample is from the 213-m (700-ft) level of the Avery Island mine and was prepared in 1984.

On the basis of these data, it is probably reasonable to conclude that variation depicted in Figure 4-1 for the Palo Duro salt cannot be attributed to differences in load frames. A serious problem depicted in Figure 4-3 is the large experimental variability found in samples which are mineralogically identical and very nearly pure halite.

Even though different load frames are not thought to introduce variability, the specimens were assigned to load frames based on nominal impurity content so that any load frame effect might be distributed among the different impurity contents. The test machine assignments are given in Table 4-1. This assignment of specimens to load frames distributes any load frame variability among nominal impurity levels so that the conclusions of this study are not influenced by differences in load frames.

The exponential-time creep law was fitted to the axial strain versus time curves for each of the successful tests. This law has the following form:

$$\varepsilon = \dot{\varepsilon}_{ss} t + e_a \{1 - \exp[-\xi t]\} \qquad (4\text{-}1)$$

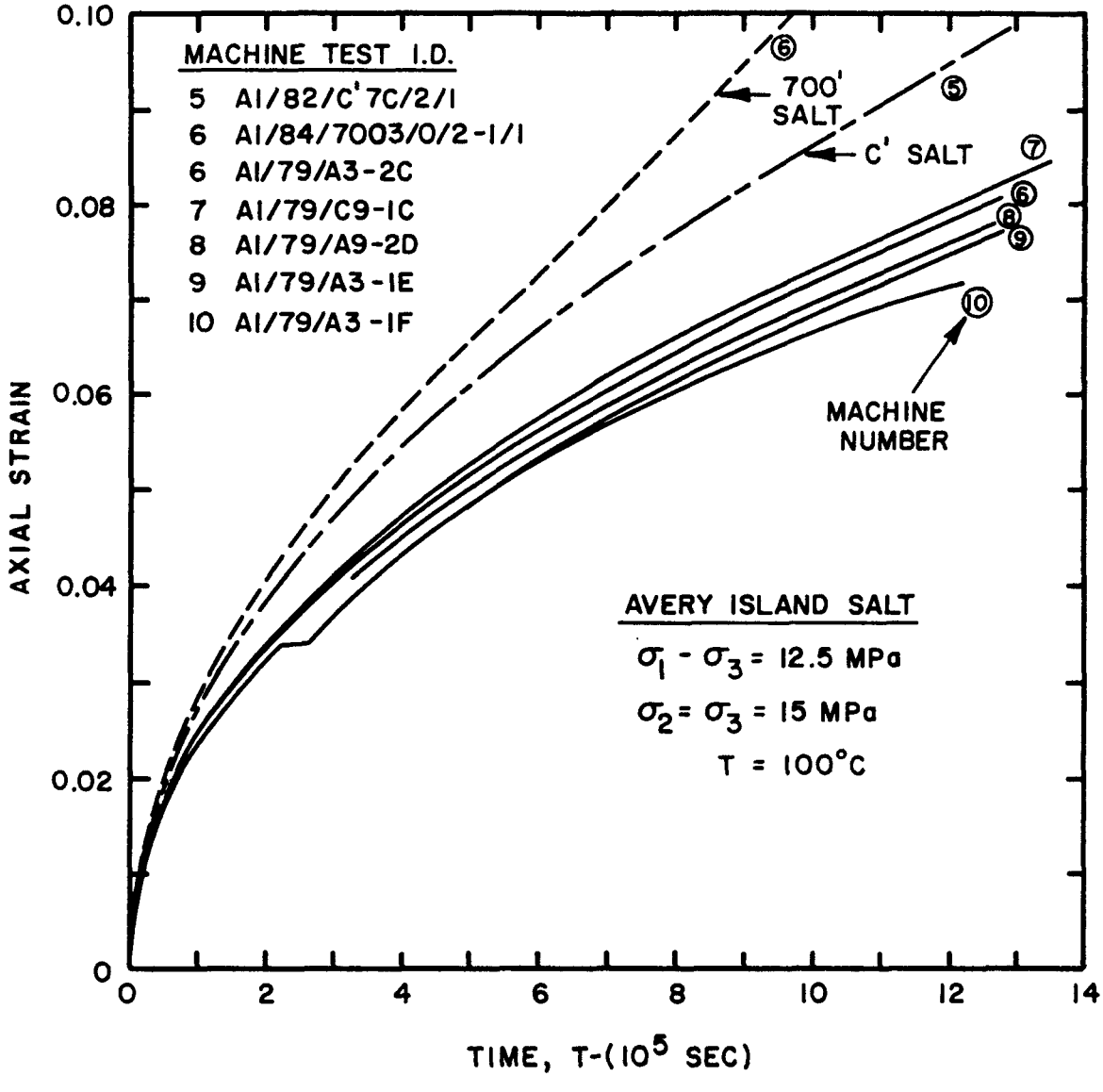

Figure 4-3. Axial Strain Versus Time Curves for Avery Island Salt: Machine Verification Tests

Table 4-1. Exponential-Time Parameter Values

Specimen ID	Depth (m)	Nominal Impurity Content	$\dot{\varepsilon}_{ss}$ (a) ($\times 10^{-9} s^{-1}$)	e_a (a) ($\times 10^{-3}$)	ξ (a) ($\times 10^{-6} s^{-1}$)	Machine Number
PE/84/WH 2450-0/1	747	Pure Salt	12.4	11.8	5.02	10
PE/84/WH 2453-0/1	748	Pure Salt	8.1	11.3	3.67	9
PE/84/WH 2509-0/1	765	Pure Salt	16.5	38.1	4.63	8
PE/84/WH 2383-0/1	726	10% Anhydrite	12.1	9.8	5.03	5
PE/84/WH 2448-0/1	746	10% Anhydrite	4.9	5.6	5.56	7
PE/84/WH 2468-0/1	752	10% Anhydrite	10.4	16.2	4.08	9
PE/84/WH 2376-0/1	724	10% Mud	13.1	14.5	2.94	10
PE/84/WH 2443-0/1	745	10% Mud	13.3	11.0	4.73	6
PE/84/WH 2464-0/1	751	10% Mud	(b)	(b)	(b)	7
PE/84/WH 2570-0/1	783	20% Mud	8.9	9.1	4.98	5
PE/84/WH 2578-0/1	786	20% Mud	12.3	17.7	5.45	6
PE/84/WH 2655-0/1	809	20% Mud	11.5	10.5	4.31	8

(a) See Equation 4-1.
(b) Jacket Failure.

where

ε = creep strain

$\dot{\varepsilon}_{ss}$ = the steady-state creep rate

t = time

e_a = an integration constant corresponding to the asymptotic transient strain

ξ = rate parameter

Table 4-1 gives the fitting parameter values obtained for each test. These values will be used in the next section to examine the influence of impurities.

The duration of the tests is too short to provide fitting parameter values that can be used to determine constitutive parameter values. Figure 4-4 plots the fitting parameter values as a function of test duration for one of the tests performed for this study. The parameter values are normalized by dividing by the value obtained at the end of the test, i.e., when all the data are fitted. Parameter values at intermediate times are determined by fitting only the data recorded before those times.

The plot shows that two of the fitting parameters decrease initially with increasing test duration, whereas the third parameter increases with increasing duration. To obtain reliable values for constitutive modeling, it is necessary to run tests long enough so that the values of the fitting parameters do not change with test duration. Note that the values of ξ are still changing rapidly, but the values of $\dot{\varepsilon}_{ss}$ and e_a are closely estimated by these data.

4.2 IMPURITIES

Impurity content has been measured by three methods in addition to the initial visual estimates: (1) X-ray fluorescence (XRF), (2) wet chemistry, and (3) point counting. Each method has advantages and disadvantages. The primary reason for measuring the composition of the samples is to determine the effect (if any) of impurity content on mechanical results, such as creep rate. Some variability is expected

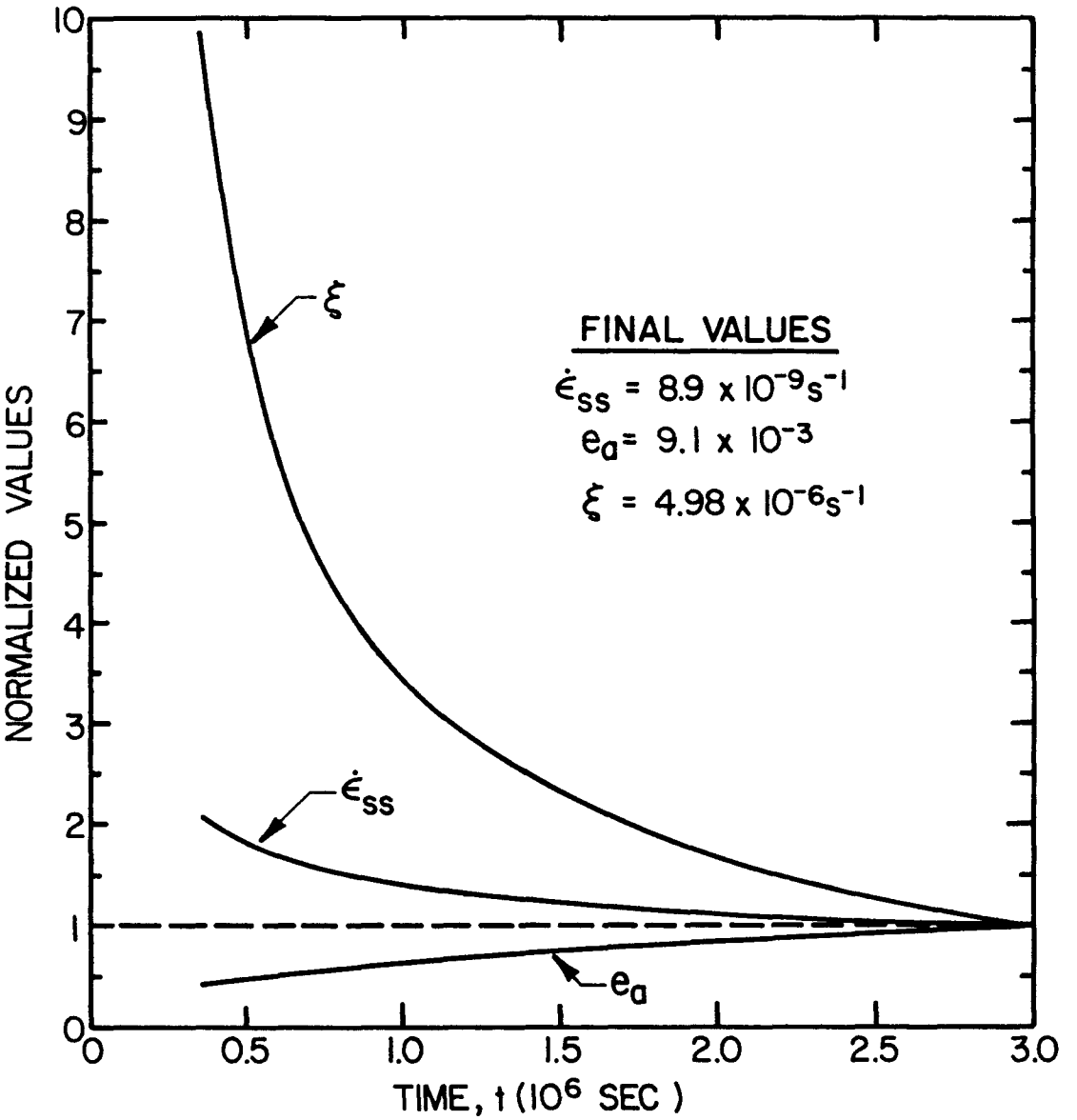

Figure 4-4. Scalar Creep Law Parameters Plotted as a Function of the Test Duration

between the different methods of analysis for a given specimen because of the heterogeneity of the sample itself.

For the purposes of this basic study, the techniques of wet chemistry and point counting, when considered together, are good measures of the impurity contents. XRF is marginal for quantitative analysis but has the advantage of quickness and scans the outer surface of the complete sample. Visual estimates are useless for quantitative purposes.

The samples used in the 11 successful tests vary widely in amounts of impurities. The primary constituents are halite, anhydrite, and clay. Natural rock salt also contains fluid films on grain boundaries and fluid inclusions within grains which can be measured optically on polished sections. Although water content coupled with the nature of deformation (e.g., dilatant versus nondilatant) has been shown to be important to mechanical response of salt [Urai et al., 1986], its study is beyond the scope of this work. The quantitative study of water content is itself very complicated [e.g., Roedder and Bassett, 1981] and to be studied adequately, the experimental matrix would have to be designed from the beginning for the specific purpose of studying water.

The composition of each tested specimen is summarized in Table 4-2. Except for the clay-rich samples, the range in impurity content is typical of natural bedded salts. The first nine samples in Table 4-2 are from the Unit 5 salt of the Palo Duro stratigraphy. Average compositions determined from wet chemistry and point counting are halite = 93.5 ± 2.5 percent, anhydrite = 4.1 ± 2.0 percent, and clay = 2.4 ± 2.5 percent. These impurity contents are indistinguishable from 25 other measurements made on Palo Duro salt. The other 25 samples for which compositions are known were tested to evaluate constitutive parameters. In summary, the heterogeneity of the samples used to evaluate the effects of impurities is almost exactly the same as the heterogeneity of samples used for constitutive law development.

The halite contents (Table 4-2) determined by wet chemistry and point counts agree closely. Duplicate runs of two wet chemistry analyses had a variation of sodium content of 3 percent. Point-to-point heterogeneity can be much greater than 3 percent, which is why large bulk samples or complete cross sections are preferred for analysis. On

Table 4-2. Impurity Content of Specimens (Weight Percent)

Specimen ID	Nominal			XRF			Wet Chemistry			Point Count		
	NaCl(a)	An(b)	Clay	NaCl	An	Clay	NaCl	An	Clay	NaCl	An	Clay
PE/84/WH2450-0/1	100	0	0	89.38	2.04	8.66	96.85	2.43	0.72	95.55	4.45	0.00
PE/84/WH2453-0/1	100	0	0	91.80	2.82	5.38	95.80	3.69	0.51	93.59	6.18	0.24
PE/84/WH2509-0/1	100	0	0	75.69	2.23	22.16	96.05	3.69	0.26	97.17	2.71	0.12
PE/84/WH2383-0/1	90	10	0	92.51	1.83	5.67	94.54	4.09	1.37	94.51	2.16	3.33
PE/84/WH2448-0/1	90	10	0	88.72	6.79	4.41	89.97	7.68	2.35	92.38	6.56	1.06
PE/84/WH2468-0/1	90	10	0	83.11	2.75	14.15	93.31	5.52	1.17	91.11	7.48	1.41
PE/84/WH2376-0/1	90	0	10	91.35	0.92	7.78	93.95	2.84	3.21	91.37	1.88	6.75
PE/84/WH2443-0/1	90	0	10	92.18	0.85	6.95	91.37	3.35	5.28	88.07	3.47	8.46
PE/84/WH2464-0/1	90	0	10	86.41	<0.51	13.09	94.17	0.77	5.06	(c)	(c)	(c)
PE/84/WH2570-0/1	80	0	20	69.26	2.75	28.05	79.59	12.92	8.49	75.13	2.09	22.78
PE/84/WH2578-0/1	80	0	20	68.93	1.53	29.47	78.16	5.61	16.23	73.03	3.51	23.46
PE/84/WH2655-0/1	80	0	20	70.41	2.04	27.46	76.17	5.96	17.87	66.92	1.54	31.54

(a) Halite.
(b) Anhydrite.
(c) Test with jacket leak not point counted.

average, less than 1 percent variation (of total weight percentage) exists between the data determined by wet chemistry and point counts for the first eight experiments.

The actual content of clay minerals is somewhat difficult to determine visually and is almost always overestimated. Visually, dark mineral content is naturally overestimated. The difficulty with clays in halides is that the so-called "clays" are mixtures of clay and other minerals, e.g., halite and anhydrite. This problem is resolved by wet chemistry in concert with ethylene diaminetetraacetic acid (EDTA) analysis (see Section 3.6.1). Clays and some anhydrite are contained in the undigested residuals after wet chemistry. The EDTA process dissolves the remaining anhydrite leaving only clay minerals and perhaps some quartz. Therefore, the percentage of clay determined by point counting is larger than the percentage determined by wet chemistry because the wet chemistry has removed the halite and anhydrite from the clay matrix.

It is obvious from Table 4-2 that the nominal impurity contents are not sufficiently quantitative for the purpose of relating mechanical data to impurity content. The samples estimated to be 100 percent halite contain from 3.5 to 5.0 percent anhydrite and clay. The samples estimated to be 90 percent halite and 10 percent anhydrite contain greater than 90 percent halite, considerably less than 10 percent anhydrite, and about 2 percent clays. The samples estimated to be 90 percent halite and 10 percent clay contain 92.2 percent halite, 2.2 percent anhydrite, and 5.6 percent clay. The samples estimated to contain 80 percent halite and 20 percent clay actually contain less than 80 percent halite, 5.2 percent anhydrite, and from 15 to 25 percent clays. In general, the visual estimates are as good as can be expected but lack the accuracy needed for the analysis of concern here. The first nine samples listed in Table 4-2 have an average mineralogy that is nearly identical with 25 other samples of salt from Units 4 and 5 of the Palo Duro Basin.

4.3 MICROPROCESSES

It is well known from metallurgy that certain types of impurities may weaken or strengthen crystalline solids. However, it is also

possible that visible impurities may not affect the strength and creep behavior of salt in any consistent and predictable way. Deformation in these creep experiments occurs by nondilatant plasticity accommodated within the crystal structure. In this study, the substructures of the deformed samples have been examined to evaluate the deformation mechanisms. The purposes of this part of the study are (1) to determine the microprocesses governing the strain-time response in each creep experiment and (2) to compare the substructures developed at various levels of strain. Different types, amounts, and arrangements of impurities might be expected to effect the microprocesses by which creep proceeds.

Typical natural salt has an "initial" substructure which includes large subgrains and a dislocation density of the order of $1.0 \times 10^{7} cm^{-2}$. Typical substructures of several natural salts - both deformed and undeformed - have been presented previously [Carter et al., 1982; Carter and Hansen, 1983; Hansen, 1985]. These previous observations help guide the conclusions drawn here.

Studies of microprocesses are made using an optical microscope and etched cleavage chips. The chips are made by disaggregating a sample and then cleaving the individual crystals along {100} (Miller indices) planes, which are perfect cleavage planes in halite. Before the cleavage chips can be studied under the microscope, they must be etched to highlight the substructural arrangement of dislocations. Etching is accomplished by holding a chip in a tweezers and agitating mildly for about 5 seconds in a solution of methanol saturated with lead chloride ($PbCl_2$). The chip is immediately rinsed in butanol for another 5 seconds and is then dried in air. About 10 or 12 chips are sufficient to study the substructure. The chips are mounted on a petrographic slide using modeler's clay and a press that sets the face of the cleavage chip flat.

Each chip is studied in detail using reflected light and magnification up to 1,800. Because the various deformation mechanisms leave different substructures, the observations are often more qualitative than quantitative. Of particular importance are the density of dislocations and any systematic arrangement they have. For example, glide of dislocations along a particular crystallographic plane will be highlighted by sharp, straight etch-pit patterns that can be oriented to give the

indices of the glide plane. Subgrains, on the other hand, can be inversely related to stress difference and taken as evidence for dislocation climb. Identification of the mechanisms is important for proper evaluation of mechanical data.

One important fact of optical microscopy is that observable substructural changes require that a percent or two of strain be imparted to the specimen. In these impurity studies, total axial strains of the successful tests range from 0.02 to 0.09. (One experiment suffered a jacket leak which gave rise to abnormally high axial strain.) Large differences in total strain, such as experienced in this suite of experiments, could be expected to cause large variations in the substructures. Samples were studied in sequence from the least axial strain (ε_1) to the greatest axial strain to evaluate evolution of substructure. The composition reflects an average between wet chemistry and point-count determinations. The observed substructures are discussed below.

WH2448-0/1; ε_1 = 0.02; Composition (Wt.%): Halite, Anhydrite, Clay = 91.18, 7.12, 1.71. Seven chips were prepared and etched. Two of the seven chips contain numerous wavy slip bands oriented along the dodecahedral plane. Spacing between glide bands is uniformly 4.5 μm. In the other five chips, glide bands are poorly developed and few in number. The five chips without many glide bands contain a considerable amount of anhydrite which suggests the absence of well developed slip lines is related to the presence of the anhydrite impurities. Qualitative variations in deformational processes can be seen within a single crystal, i.e., a single etched cleavage chip. On the clean, clear end of a chip, dislocation density is $4.4 \times 10^7 cm^{-2}$, while on the end with considerable anhydrite, the density is $3.6 \times 10^7 cm^{-2}$.

WH2570-0/1; ε_1 = 0.035; Composition (Wt.%): Halite, Anhydrite, Clay = 77.36, 7.50, 15.64. Eight chips were prepared from this sample: five from halite zones within the sample and three from halite grains apparently floating in a clay matrix. All of the grains have similar substructures so distinction of deformational processes cannot be made on the basis of surrounding material. In other words, the clay matrix transmits stresses to the isolated halite crystals effectively. Substructures in this sample are characterized by glide bands (Figure

4-5). The glide bands are usually spaced 4.5 μm apart and are almost always present in pairs, as exhibited in Figure 4-5. A theoretical explanation for the development of pairs has not yet been put forth. Whatever the source, the glide pairs are not restricted by crystallography, although in Figure 4-5 the glide pairs are essentially parallel {110}. Figure 4-5 also shows polygonization and reduction of dislocation density in the vicinity of fluid inclusions, which are the small black cubes in the photomicrograph. Carter et al. [1982] earlier postulated that moisture in the halite crystal structure enhances diffusion. Apparently, as seen in Figure 4-5, the dislocations are arranging into polygons while simultaneously reducing the free dislocation density in the proximity of the fluid inclusions.

WH2453-0/1; ε_1 = 0.035; Composition (Wt.%): Halite, Anhydrite, Clay = 94.69, 4.94, 0.39. The substructure of this sample contains wavy slip bands and an associated high dislocation density. Between wavy slip lines are augen-shaped cells which are essentially free of dislocations. The cell size is approximately 4.5 μm, which corresponds identically to the distance between glide pairs, as noted above. These cellular structures may be mistaken for polygons. Cells between wavy glide bands are much smaller than the equilibrium size of steady-state polygons. For comparison, the steady-state polygon size at 15 MPa is 13 μm [Carter and Hansen, 1983, Table 15].

WH2655-0/1; ε_1 = 0.045; Composition (Wt.%): Halite, Anhydrite, Clay = 71.55, 3.75, 24.71. The substructure of this sample consists entirely of wavy slip. In general, the spacing between glide bands remains 4.5 μm and all chips are completely thatched with intersecting glide bands on orthogonal dodecahedral planes. The substructure in this sample is very similar to the previously described substructures at a strain of 0.035. Once again, cellular structures that look like subgrains are formed between wavy glide bands. In this sample, the cells are square, 4.5 by 4.5 μm, and therefore distinguishable from steady-state polygons by both shape and size.

WH2383-0/1; ε_1 = 0.045; Composition (Wt.%): Halite, Anhydrite, Clay = 94.52, 3.12, 2.35. Seven chips were etched and each chip exhibits complex, interwoven wavy slip planes. Cellular structures exist between bands (Figure 4-6). The wavy glide system comprises several

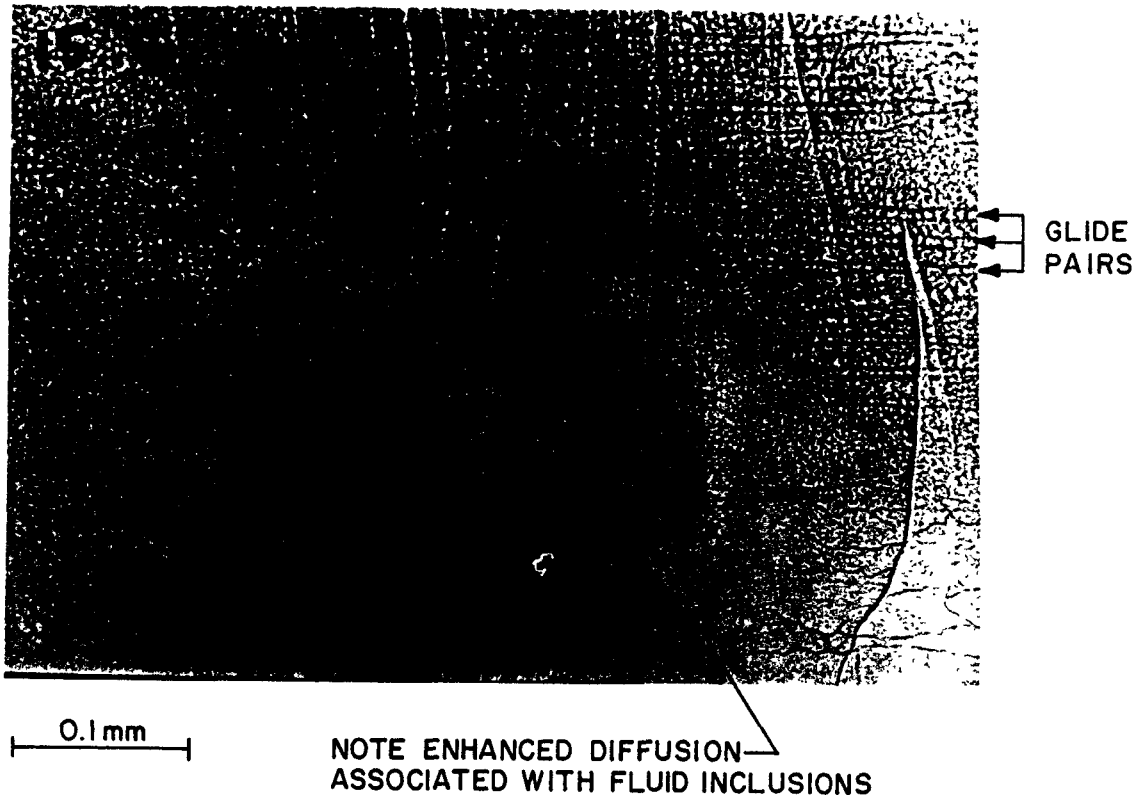

Figure 4-5. Substructure of WH2570-0/1; $\varepsilon_1 = 0.04$, $T = 75°C$, $\sigma_1 - \sigma_2 = 15$ MPa, $\sigma_2 = \sigma_3 = 15$ MPa

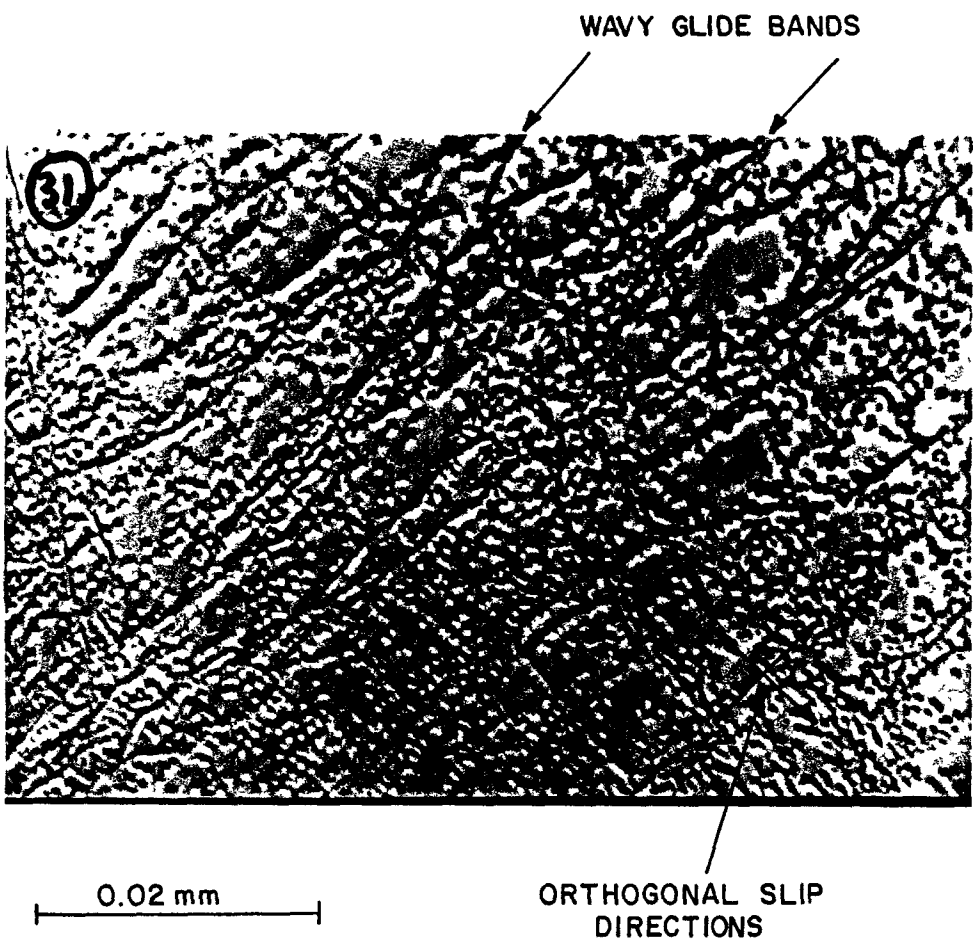

Figure 4-6. Substructure of WH2383-0/1; ε_1 = 0.05, T = 75°C, $\sigma_1 - \sigma_2$ = 15 MPa, $\sigma_2 = \sigma_3$ = 15 MPa

distinct bands which take on the same wavy shape. A secondary orthogonal system can also be seen in the photomicrograph (Figure 4-6).

WH2468-O/1; ε_1 = 0.047; Composition (Wt.%): Halite, Anhydrite, Clay = 92.12, 6.50, 1.29. Eight chips were etched. The most significant substructural artifacts are wavy glide planes and high dislocation density (Figure 4-7).

WH2509-O/1; ε_1 = 0.085; Composition (Wt.%): Halite, Anhydrite, Clay = 96.61, 3.20, 0.19. This sample suffered almost twice as much plastic strain as the other successful tests in this study. The substructures contain nothing to indicate that such larger strains have been induced. Typically, spacing between the wavy bands is an average of 4.5 μm, which is identical to measurements made at axial strains of 0.035, 0.045, and 0.047. This sample does contain some polygonized areas which, again, are found to be associated with fluid inclusions consistent with the hypothesis of enhanced diffusion [Carter et al., 1982].

WH2464-O/1; $\varepsilon_1 > 0.10$ (Creep Rupture); Composition (Wt.% Wet Chemistry Only): Halite, Anhydrite, Clay = 94.17, 0.77, 5.06. The substructure is the same as that found in samples deformed to 3.5 and 4.5 percent strain; i.e., it consists of distinct, singular wavy slip bands. The bands are separated by 4.5 μm and occasionally cross-link to present the appearance of polygons. This substructure was probably produced during the initial deformation ($\varepsilon_1 < 0.03$) before the jacket leak. Following the jacket leak, the axial strain rate accelerated and continued to about 0.10. The accelerating creep resulted from microcracking principally along grain boundaries oriented parallel to the maximum principal stress. Cracking is made evident by epoxy impregnation. The brittle mechanism of grain-boundary cracking completely dominates creep following the jacket leak so the plastic substructure is frozen at the 0.03 strain level.

When all of the etched cleavage chips for a sample are considered together, the major conclusion regarding microdynamics is that the amount and mineral species of the impurities had no optically observable influence on the substructure. The controlling creep mechanism for all of the tests is glide aided by cross slip. Wavy glide bands are evident in every sample regardless of the amount of strain. In a few cases,

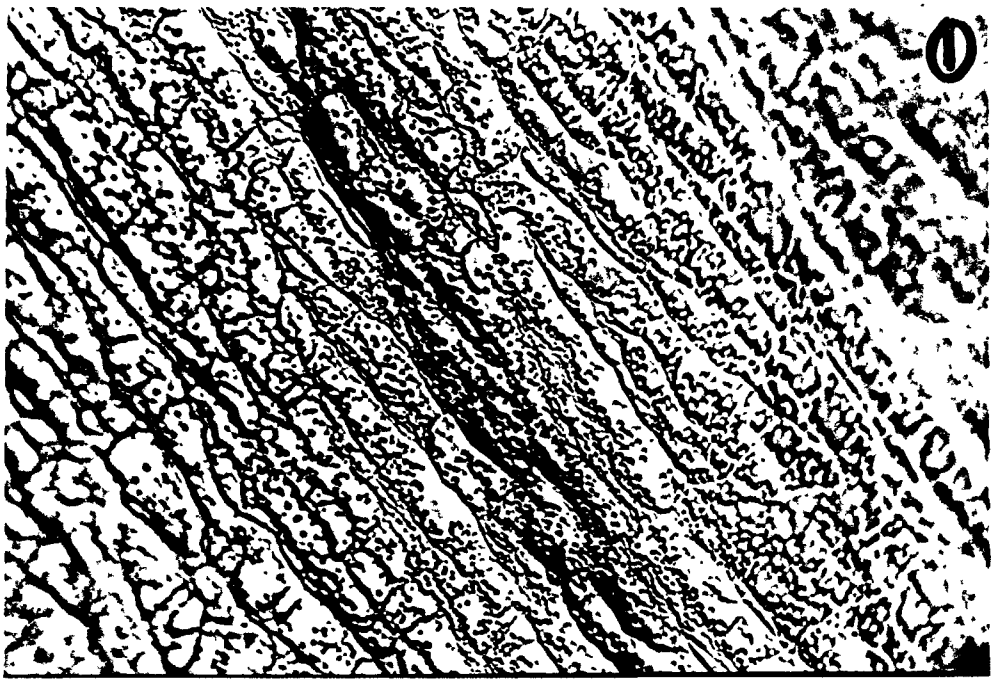

Figure 4-7. Substructure of WH2468-0/1; $\varepsilon_1 = 0.05$, $T = 75°C$, $\sigma_1 - \sigma_2 = 15$ MPa, $\sigma_2 = \sigma_3 = 15$ MPa

dislocation motion is apparently impeded by anhydrite (most probably by excess Ca^{++} in the halite crystal structure). But, for the vast majority of etched cleavage chips examined, the cross-slip process is evident at relatively small strain (0.02).

Two noteworthy observations are in order: (1) in the vicinity of fluid inclusions, free dislocation is low and subgrains are often well developed and (2) halite grain deformation within each sample is uniform. The first observation concurs with earlier observations of Carter et al. [1982]. The observed result of enhanced diffusion is a marked reduction in dislocation density and localized polygonization. Uniformity of deformation within the halite occurs even if the individual grains are surrounded by clay. The clays in these clay-rich samples tend to be disseminated rather than in seams. Halite crystals isolated in localized clay zones contain the exact same substructure as halite grains surrounded by more halite.

Missing Page
from
Original Document

5.0 ANALYSIS

The effects of impurities are evaluated by linear regression analysis between each mechanical measurement and the weight percentages of the mineral constituents. To assist in visualizing the calculated relationships, plots of mechanical results versus mineral species are given in Appendix C. The mechanical data include calculated values of steady-state strain rate ($\dot{\varepsilon}_{ss}$), asymptotic transient strain (e_a), a rate parameter (ξ), and total strain at the termination of the test (ε_1). Mineralogy is subdivided into halite, anhydrite, and clay. Table 5-1 summarizes all the data to be correlated.

The mineral percentages are an average from the results of wet chemistry and point counts. As each method is estimated to be of equal validity and has about the same accuracy, an average of the weight percentages is the best quantity to use. The mechanical results (except total strain) come from fits to each strain-time curve individually. As such, they represent a three parameter fit to the curve and duplicate the test data accurately. They are fit for curves of equal duration and thereby provide quantities that can be compared between tests and correlated with other quantities. The three mechanical data points also have a physical interpretation. The steady-state strain rate is the best estimate of the steady state to the point of termination. It does not mean that it is a true and absolute value, only that it is a quantity that can be measured for each test over identical stresses, temperature, and time. The same arguments hold for the asymptotic transient strain and the rate parameter. They are quantifiable values that approximate the amount of transient strain and the time required to reach steady state. The three parameters are calculated similarly for each test and quantify the primary characteristics of each curve for as long as the test was run.

The lower half of Table 5-1 summarizes all of the correlation coefficients between mineralogy and mechanical results. These correlation coefficients can be calculated on any hand calculator that has a linear regression routine. Interpretation of correlation coefficients is somewhat subjective. Basically, a strong relationship would have a

Table 5-1. Correlation of Mechanical Results and Impurity Content

Correlated Parameters	Test Identification Depths (ft)										
	2,450	2,453	2,509	2,383	2,448	2,468	2,376	2,443	2,570	2,578	2,655
Halite (Wt.%)	96.2	94.7	96.6	94.5	91.2	92.2	92.7	89.7	77.4	75.6	71.6
Anhydrite (Wt.%)	3.4	4.9	3.2	3.1	7.1	6.5	2.4	3.4	7.5	4.6	3.8
Clay (Wt.%)	0.3	0.4	0.2	2.4	1.7	1.3	5.0	6.9	15.6	19.9	24.7
$\dot{\varepsilon}_{ss}$ $(10^{-9}s^{-1})$	12.4	8.1	16.5	12.1	4.9	10.4	13.1	13.3	8.9	12.3	11.5
ε_a (10^{-3})	11.8	11.3	38.1	9.8	5.6	16.2	14.5	11.0	9.1	17.7	10.5
ξ $(10^{-6}s^{-1})$	5.0	3.7	4.6	5.0	5.6	4.1	2.9	4.7	5.0	5.5	4.3
ε_1 [@ $3(10^6 s)$]	4.8	3.5	8.6	4.5	2.0	4.7	5.3	5.0	3.5	5.3	4.5

Mineral Content	Mechanical Results			
	$\dot{\varepsilon}_{ss}(10^{-9}s^{-1})$	$e_a(10^{-3})$	$\xi(10^{-6}s^{-1})$	ε_1
Halite (Wt.%)	0.13	0.24	-0.24	0.19
Anhydrite (Wt.%)	-0.78	-0.34	0.37	-0.61
Clay (Wt.%)	0.02	-0.18	0.17	-0.08

Correlation Coefficients

correlation coefficient approaching 1.00 and a random set of data would have a correlation coefficient near 0.00. The figures in Appendix C will assist in evaluation of the significance of each correlation coefficient in Table 5-1.

Only two moderate correlations exist: (1) between anhydrite content and steady-state strain rate (-0.78) and (2) between anhydrite content and total strain (-0.61). That means greater percentages of anhydrite content systematically reduces the rate and amount of creep. All other correlations are statistically insignificant, which means that no relationship exists within this set of data between the creep parameters and the mineralogical composition. Therefore, the remainder of this analysis will concentrate on the steady-state parameter, particularly as it relates to the anhydrite content.

An estimate of a steady-state creep rate ($\dot{\varepsilon}_{ss}$) has been made for each experiment (see Table 4-1). Estimates of $\dot{\varepsilon}_{ss}$ for the 11 successful experiments range from 4.9 to 16.5 x $10^{-9}s^{-1}$, a difference of more than a factor of three. This is well within the range of various natural salts, such as plotted in Figure 4-2 ($5 \times 10^{-9}s^{-1} < \dot{\varepsilon}_{ss} < 23 \times 10^{-9}s^{-1}$). The composition of the sample with the fastest creep rate (PE/84/WH2509-0/1) is not unusual; i.e., the weight percentages of halite, anhydrite, and clay = 96.6, 3.2, and 0.2, respectively. Another sample (PE/84/WH2453-0/1) with almost exactly the same composition has a steady-state rate that is slower by a factor of two.

If the rates differ by a factor of two for samples of nearly identical composition, what can be said quantitatively about samples whose compositions vary greatly? Consider grouping the samples into Unit 5 (94 percent halite) and Unit 4 (less than 80 percent halite) and plotting steady-state strain rate versus halite content (Figure 5-1). The spread of steady-state creep rates is larger in the clean salts than in the clay-rich salts, perhaps because of the larger number of tests. On average, the steady-state strain rate is 11.4 x $10^{-9}s^{-1}$ for the eight clean samples and 10.9 x $10^{-9}s^{-1}$ for the three dirty samples. This exercise demonstrates that, on average, very large differences in impurity content do not effect the steady-state strain rate; at the same time, samples with identical compositions can creep at steady-state rates that differ by a factor of two. Similar analyses can be made using any of the mechanical results plotted in Appendix C.

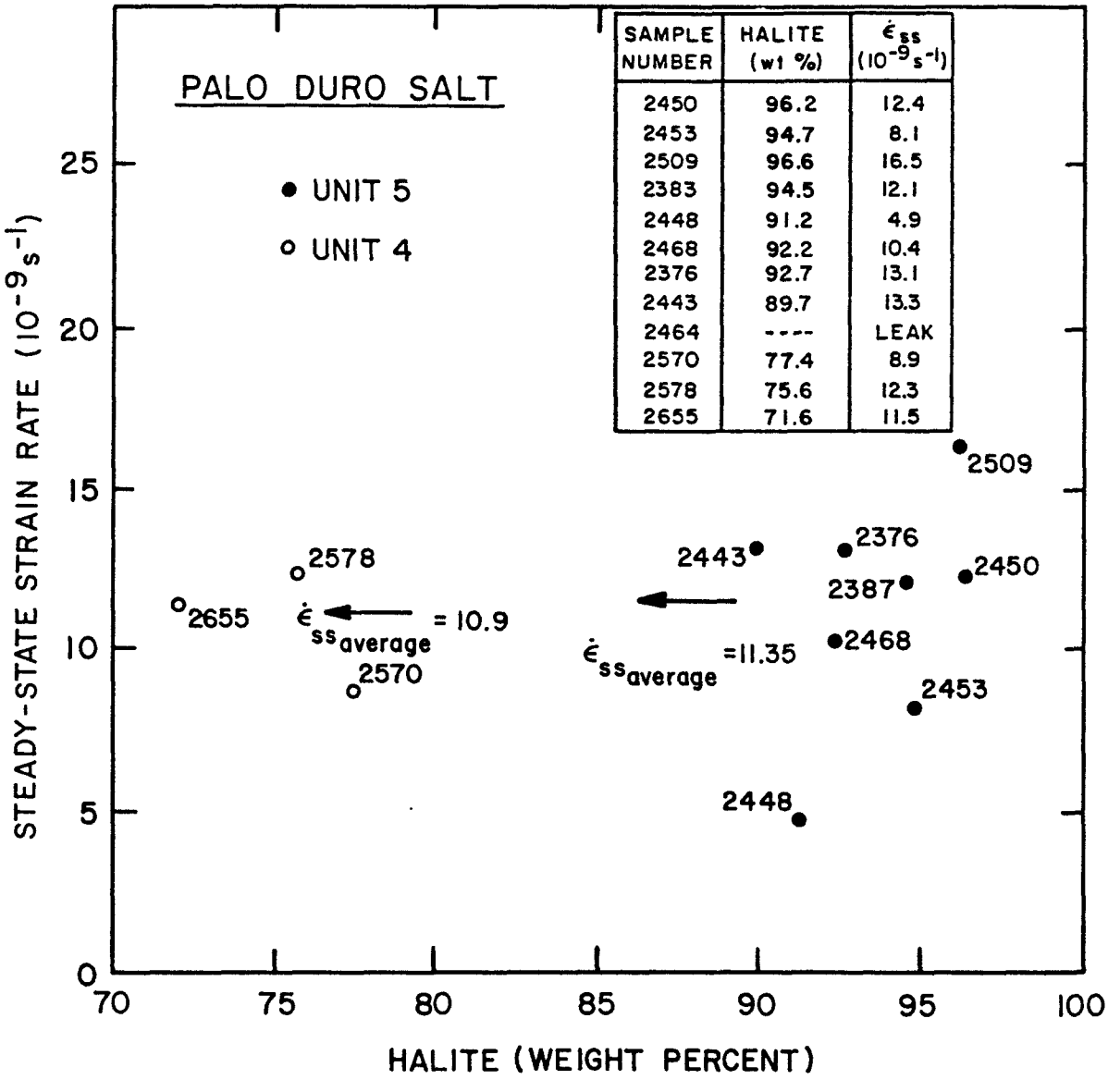

Figure 5-1. Halite Content Versus Steady-State Strain Rate

Previously a strong correlation was found between anhydrite content and creep rate when anhydrite content ranged from nearly zero to about 12 percent by weight. The more anhydrite a sample contains, the slower the creep rate and the smaller the total strain. The process by which the strengthening occurs may not result from the anhydrite itself, but rather the presence of Ca^{++} ionic defects within the NaCl crystal structure [Heard and Ryerson, 1982].

The anhydrite content and steady-state strain rates of the 11 successful creep tests are plotted in Figure 5-2. The steady-state strain rate generally increases as anhydrite content decreases. The correlation between anhydrite content and steady-state strain rate is bounded, of course. As anhydrite content becomes large, the strain rate would decrease appreciably. One constraint would be the creep rate under these conditions for a specimen of 100 percent anhydrite. But, the concern here is with expected levels of disseminated anhydrite in natural rock salt. If, for example, the steady-state strain rate of nearly pure Avery Island salt tested under identical conditions (see Figure 4-2) is superimposed on Figure 5-2, the correlation appears to be nonlinear as purity increases. Avery Island salt is more than 99 percent halite; the only impurity is less than 1 percent anhydrite. Avery Island salt also is relatively weak compared to other natural salts.

Table 5-1 summarizes the experimental results and mineralogy of each experiment. Each mineral species is correlated with each mechanical parameter. Some of these data are collinear, e.g., the fastest steady-state strain rate occurs in the same experiment as the largest axial strain. Similarly, greater percentages of halite relate to smaller percentages of impurities. Nonetheless, all of the correlation coefficients for each pair of data sets are listed in Table 5-1. The strongest correlations exist between anhydrite content and the mechanical results. (The relationship between $\dot{\varepsilon}_{ss}$ and anhydrite content is plotted in Figure 5-2.) Much weaker correlations exist between halite content and the experimental results. The weakest correlation exists between clay content and the steady-state strain rate. Extremely low correlations (0.03 in this case) indicate almost completely random relationships.

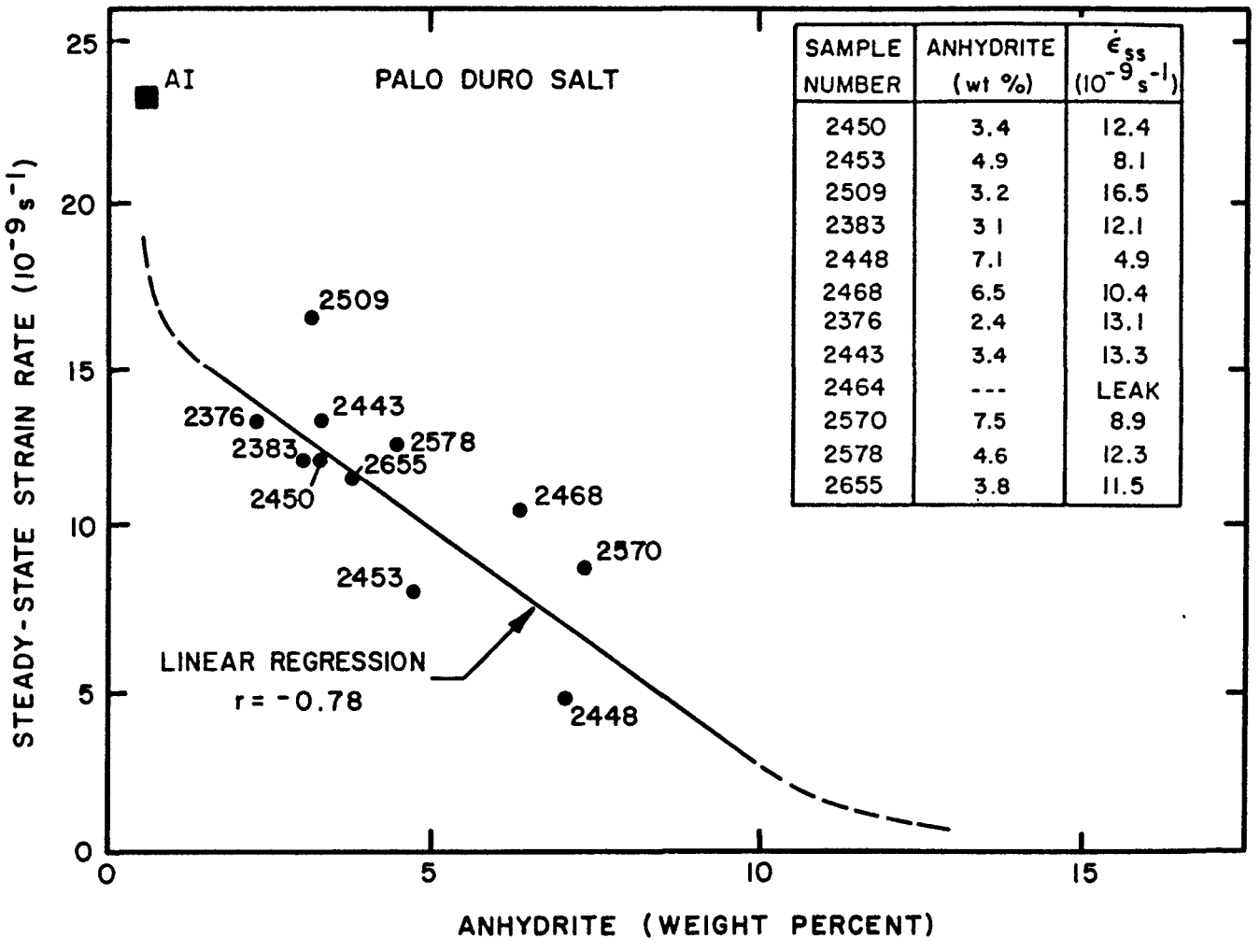

SAMPLE NUMBER	ANHYDRITE (wt %)	$\dot{\epsilon}_{ss}$ (10^{-9} s^{-1})
2450	3.4	12.4
2453	4.9	8.1
2509	3.2	16.5
2383	3 1	12.1
2448	7.1	4.9
2468	6.5	10.4
2376	2.4	13.1
2443	3.4	13.3
2464	---	LEAK
2570	7.5	8.9
2578	4.6	12.3
2655	3.8	11.5

Figure 5-2. Anhydrite Content Versus Steady-State Strain Rate

6.0 CONCLUSIONS

An experiment has been performed on salt from the Palo Duro Basin to assess the influence of impurity content on creep deformation. Twelve triaxial compression creep tests were performed on salt specimens from the Woods-Holtzclaw well. The stress difference, confining pressure, and temperature in all 12 tests were 15 MPa, 15 MPa, and 75°C (167°F), respectively. These test conditions are representative of those expected in the room region of a nuclear waste repository. The data from these tests show that the creep strains after 3×10^6s (35 days) vary by as much as a factor of four. The strain versus time data obtained from each test were fitted to the exponential-time creep law, and the three fitting parameters were evaluated. The fitting parameter values were used to evaluate the effects of impurity content.

The impurity contents estimated by visual inspection at the time the samples were selected for testing were not sufficiently accurate for quantitative calculations. Subsequent petrological studies accurately measured the halite, anhydrite, and clay within each specimen. Overall, the 12 specimens comprise 71.6 to 96.6 percent halite, 2.4 to 7.5 percent anhydrite, and 0.2 to 24.7 percent clay. Nine of the 12 specimens are similar to many other tested specimens from the Lower San Andres Unit 5. They range from 90 to 97 percent halite and average 94 percent with a standard deviation of 2 percent. The remaining 6 percent impurities are disseminated clay and anhydrite. The other three specimens from the Lower San Andres Unit 4 contain large amounts (average 20 percent) of uniformly distributed clays and average only 75 percent halite.

This evaluation is limited to one set of experimental conditions. The mineral species are also limited to halite, anhydrite, and clay, although no other mineralogical species were present at the detectable levels of optical microscopy and wet chemistry. These ranges in composition are representative of natural rock salt, but the correlations (or lack of correlation) between mineral species and creep test results as determined here cannot be extrapolated with confidence to other stress and temperature regimes. For example, the influence of impurity content may change as a function of temperature and stress.

Linear regression analyses were made between each of the quantities of mineral content and each of the experimental parameters. Plots were also constructed for each combination of quantities (Appendix C). The results show almost no correlation between the experimental parameters and the quantities of mineral species (Table 5-1). Particularly, the amounts of clay and halite, considered separately, have no statistically significant correlation with the amount of transient creep, rate of steady-state creep, the rate parameter, and total strain. In fact, the experimental results appear to be independent of the amount of halite or clay. The only moderately strong correlations of experimental results and mineralogy involves an increase in creep resistance with an increase in anhydrite content. Steady-state strain rate and the amount of total axial strain (because of collinearity) are reduced as anhydrite content increases, and the correlation coefficients are -0.78 and -0.61, respectively.

It must be emphasized that these results are not conclusive evidence that the composition of the salt sample has no effect on the creep properties. These results apply to representative natural salt tested at 75°C, a stress difference of 15 MPa, and a confining pressure of 15 MPa. A further consideration is that the impurities studied were only those that are visible microscopically. Perhaps submicroscopic clusters of ions effect the behavior of salt more than the evident minerals. Another potentially important impurity is water which is naturally present in all salt but was not quantified in this study. Allowing for these caveats, anhydrite is the only impurity that systematically effects the creep of salt. The more anhydrite in a sample, the more resistant to creep the sample is.

Composition of the samples does not affect the overall microprocesses. In the vicinity of fluid inclusions, free dislocation density is lower than elsewhere in the same crystal, and the proximal substructure is polygonized subgrain arrays. Locally, the presence of anhydrite in the halite crystal appears to reduce or prevent glide processes. But by far, the preponderance of the substructures is wavy glide bands situated parallel to {110} (Miller indices). The process is evident at all levels of strain (0.02 to 0.09) encountered in this study. The rate controlling process appears to be cross slip.

7.0 REFERENCES

Carter, N. L., and F. D. Hansen, 1983. "Creep of Rocksalt," Tectonophysics, Vol. 92, pp. 275-333.

Carter, N. L., F. D. Hansen, and P. E. Senseny, 1982. "Stress Magnitudes in Natural Rock Salt," Journal of Geophysical Research, Vol. 87, No. B11, pp. 9289-9300.

Handin, J., J. E. Russell, and N. L. Carter, 1984. Transient Creep of Repository Rocks, Final Report: Mechanistic Creep Laws for Rock Salt, BMI/ONWI-550, prepared by Texas A&M Research Foundation for Office of Nuclear Waste Isolation, Battelle Memorial Institute, Columbus, OH.

Hansen, F. D., 1985. Deformation Mechanisms of Experimentally Deformed Salina Basin Bedded Salt, BMI/ONWI-552, prepared by RE/SPEC Inc. for Office of Nuclear Waste Isolation, Battelle Memorial Institute, Columbus, OH.

Heard, H. C., and F. J. Ryerson, 1982. "Rheology of Polycrystalline Halite Containing Cation Impurities," EOS, Transaction, American Geophysical Union, Vol. 63, pp. 1095.

Laul, J. C., 1984.* Letter from Laul, Pacific Northwest Laboratory, to C. Jones, Bendix Field Engineering, Grand Junction, CO, about X-ray flourescene data, July 18.

Mellegard, K. D., P. E. Senseny, and F. D. Hansen, 1983. Quasi-Static Strength and Creep Characteristics of 100-mm-Diameter Specimens of Salt From Avery Island, Louisiana, ONWI-250, prepared by RE/SPEC Inc. for Office of Nuclear Waste Isolation, Battelle Memorial Institute, Columbus, OH.

Roedder, E., and R. L. Bassett, 1981. "Problems in Determination of Water Content of Rock Samples and Its Significance in Nuclear-Waste Storage Siting," Geology, Vol. 9, pp. 525-530.

---

* This reference is reprinted in Appendix B of this report.

Senseny, P. E., T. W. Pfeifle, and K. D. Mellegard, 1985. Constitutive Parameters for Salt and Nonsalt Rocks From the Detten, G. Friemel, and Zeeck Wells in the Palo Duro Basin, Texas, BMI/ONWI-549, prepared by RE/SPEC Inc. for Office of Nuclear Waste Isolation, Battelle Memorial Institute, Columbus, OH.

Senseny, P. E., T. W. Pfeifle, and K. D. Mellegard, 1986. Exponential-Time Constitutive Law for Palo Duro Unit 4 Salt From the J. Friemel #1 Well, BMI/ONWI-595, prepared by RE/SPEC Inc. for Office of Nuclear Waste Isolation, Battelle Memorial Institute, Columbus, OH.

Urai, J. L., C. J. Spiers, H. J. Zwart, and G. S. Lister, 1986. "Weakening of Rock Salt by Water During Long-Term Creep," Nature, Vol. 324, pp. 554-557.

APPENDIX A

STRAIN VERSUS TIME DATA FOR WOODS-HOLTZCLAW SALT

Missing Page
from
Original Document

APPENDIX A

LIST OF FIGURES

		Page
A-1.	Measured Axial and Lateral Creep Strain for Palo Duro Salt Specimen PE/84/WH2450-0/1	51
A-2.	Measured Axial and Lateral Creep Strain for Palo Duro Salt Specimen PE/84/WH2453-0/1	52
A-3.	Measured Axial and Lateral Creep Strain for Palo Duro Salt Specimen PE/84/WH2509-0/1	53
A-4.	Measured Axial and Lateral Creep Strain for Palo Duro Salt Specimen PE/84/WH2383-0/1	54
A-5.	Measured Axial and Lateral Creep Strain for Palo Duro Salt Specimen PE/84/WH2448-0/1	55
A-6.	Measured Axial and Lateral Creep Strain for Palo Duro Salt Specimen PE/84/WH2468-0/1	56
A-7.	Measured Axial and Lateral Creep Strain for Palo Duro Salt Specimen PE/84/WH2376-0/1	57
A-8.	Measured Axial and Lateral Creep Strain for Palo Duro Salt Specimen PE/84/WH2443-0/1	58
A-9.	Measured Axial and Lateral Creep Strain for Palo Duro Salt Specimen PE/84/WH2464-0/1	59
A-10.	Measured Axial and Lateral Creep Strain for Palo Duro Salt Specimen PE/84/WH2570-0/1	60
A-11.	Measured Axial and Lateral Creep Strain for Palo Duro Salt Specimen PE/84/WH2578-0/1	61

APPENDIX A

LIST OF FIGURES
(Continued)

Page

A-12. Measured Axial and Lateral Creep Strain for Palo Duro Salt Specimen PE/84/WH2655-O/1 62

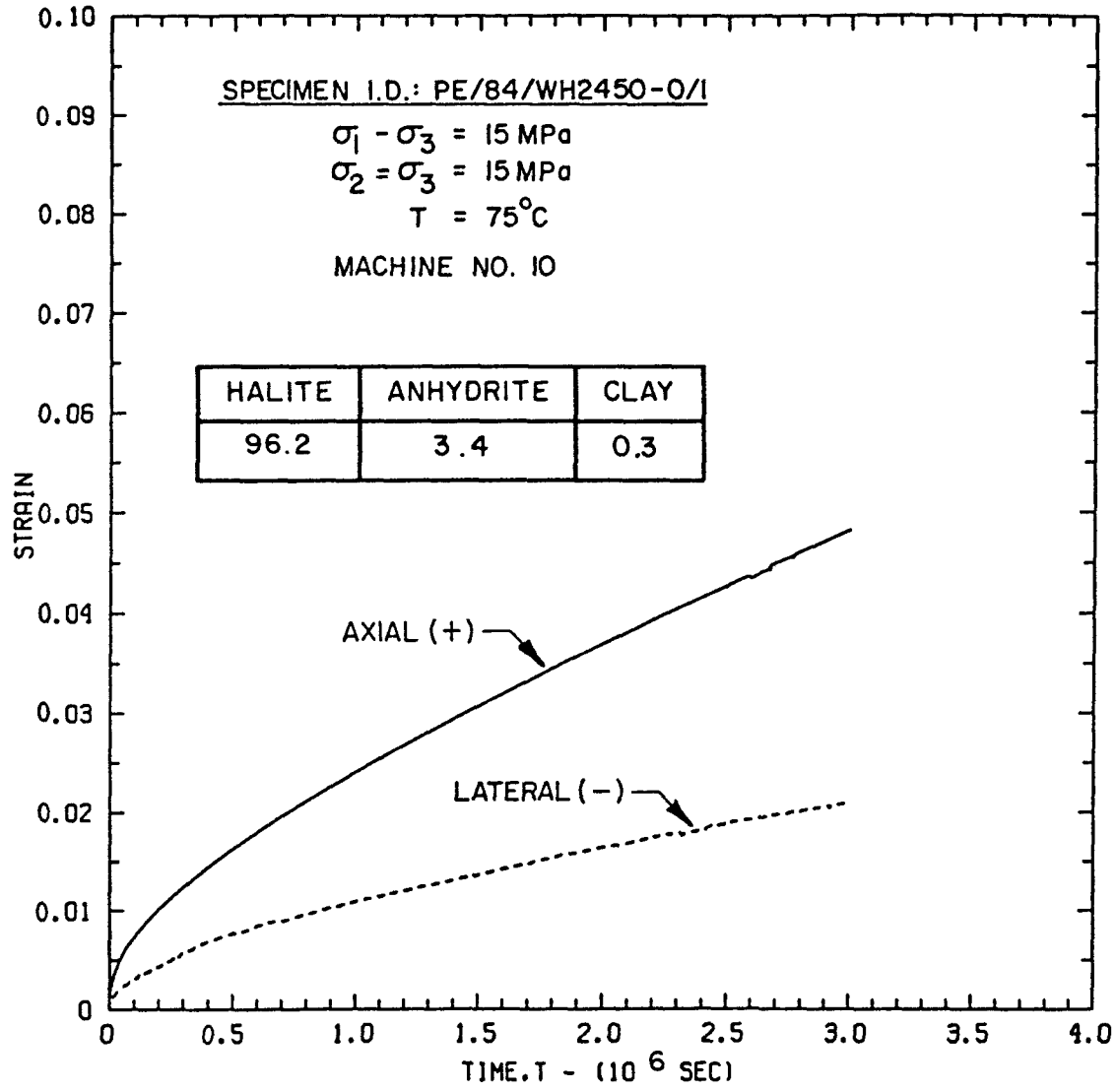

Figure A-1. Measured Axial and Lateral Creep Strain for Palo Duro Salt Specimen PE/84/WH2450-0/1

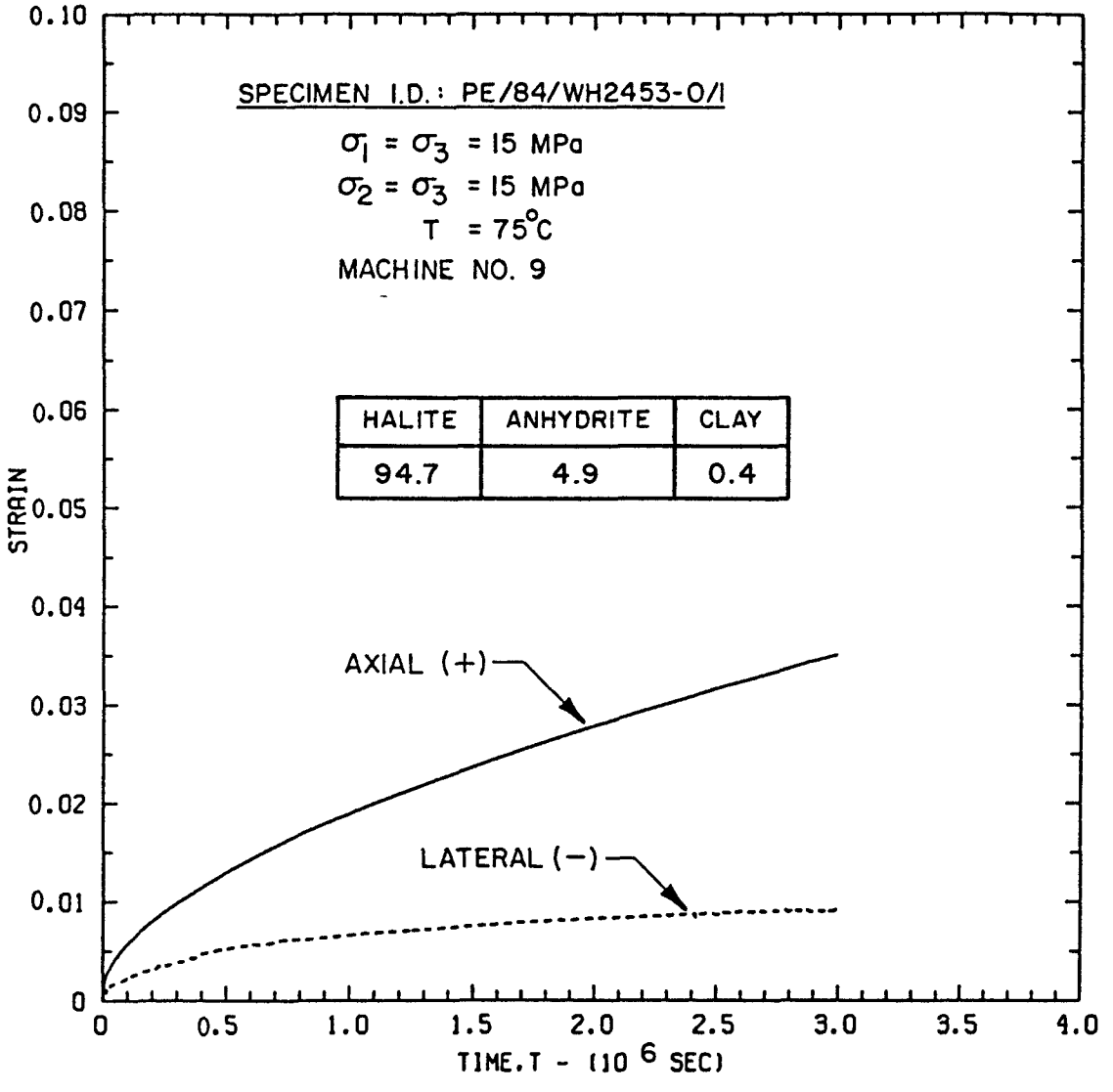

Figure A-2. Measured Axial and Lateral Creep Strain for Palo Duro Salt Specimen PE/84/WH2453-O/1

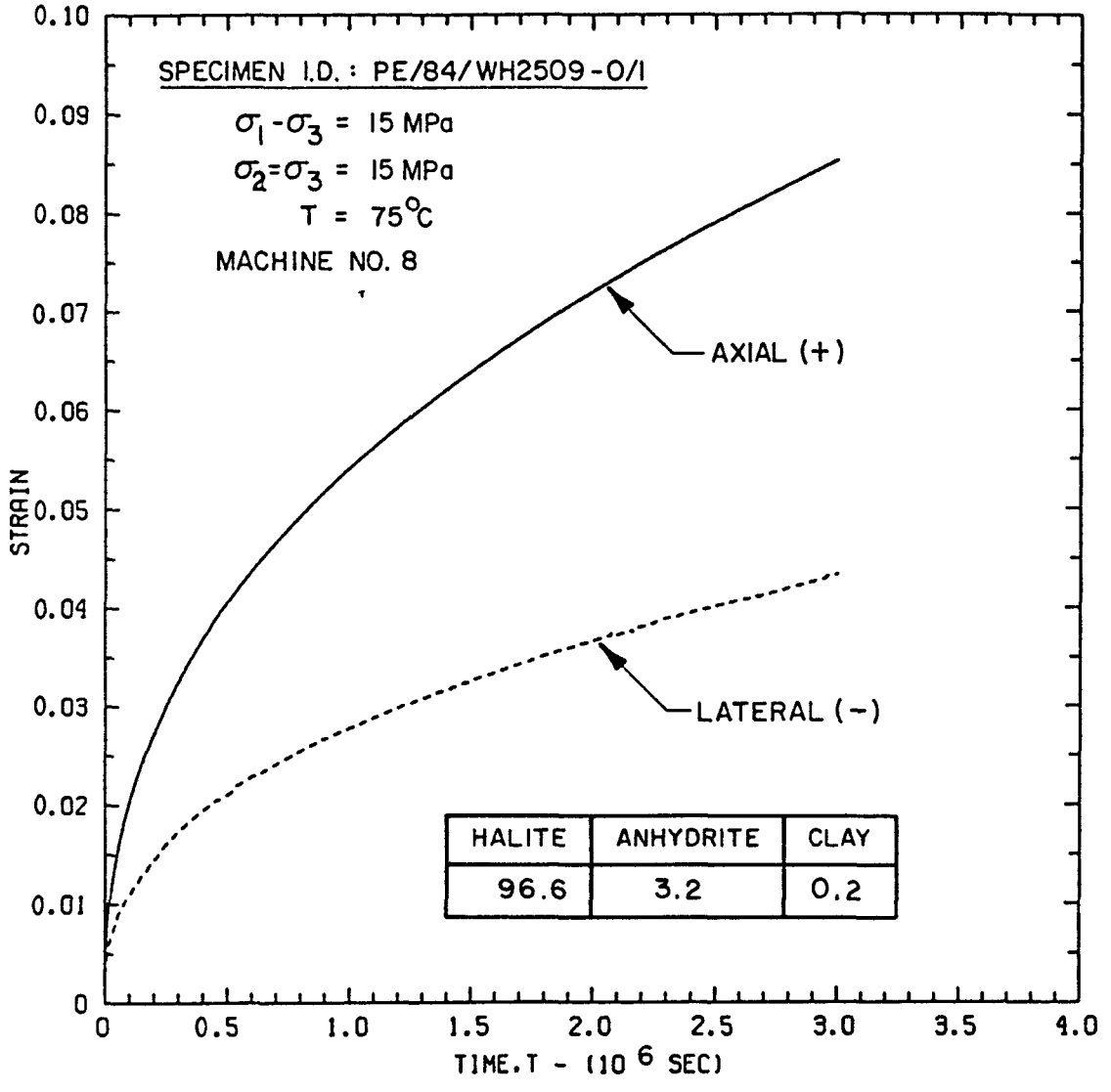

Figure A-3. Measured Axial and Lateral Creep Strain for Palo Duro Salt Specimen PE/84/WH2509-O/1

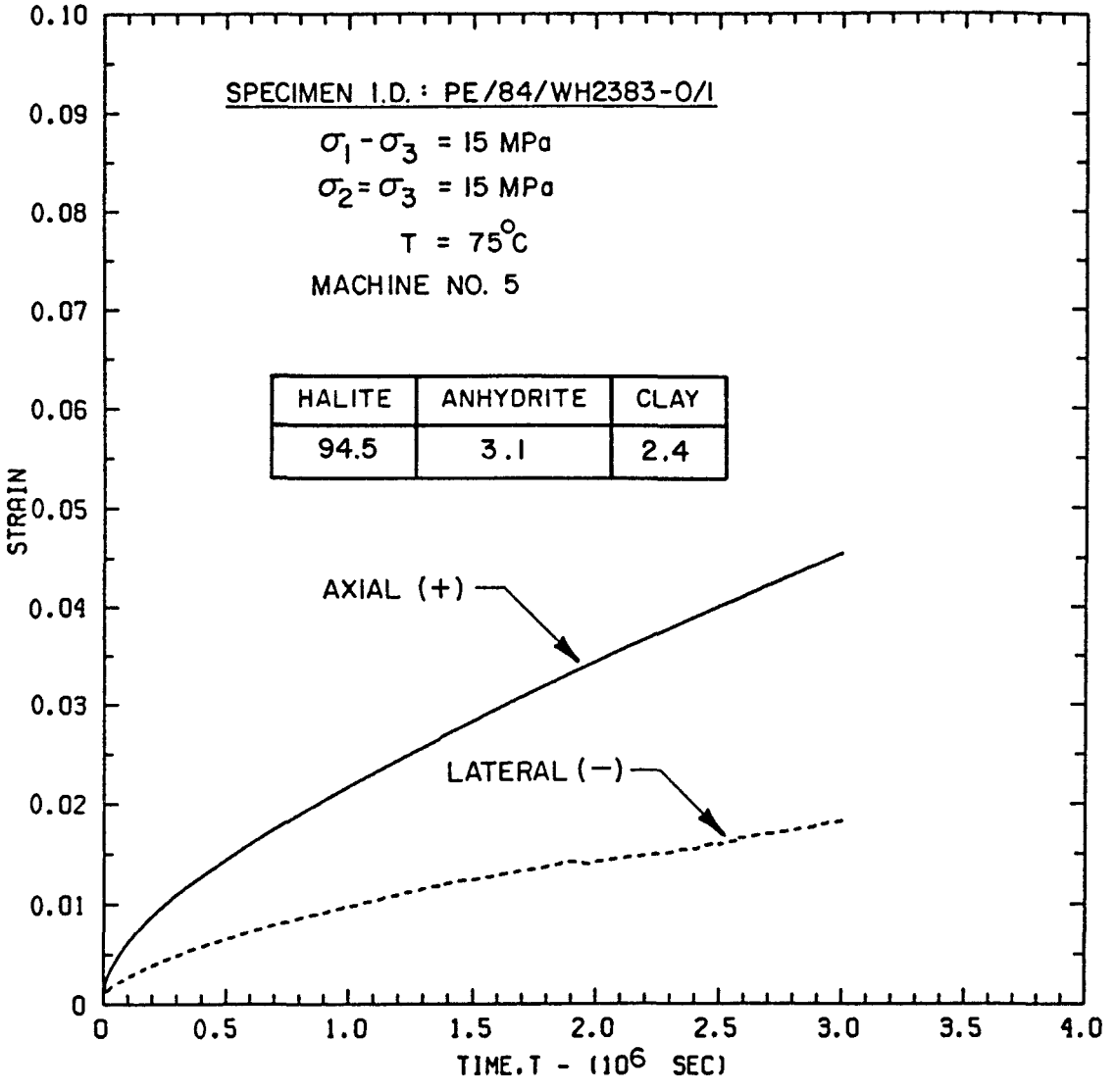

Figure A-4. Measured Axial and Lateral Creep Strain for Palo Duro Salt Specimen PE/84/WH2383-O/1

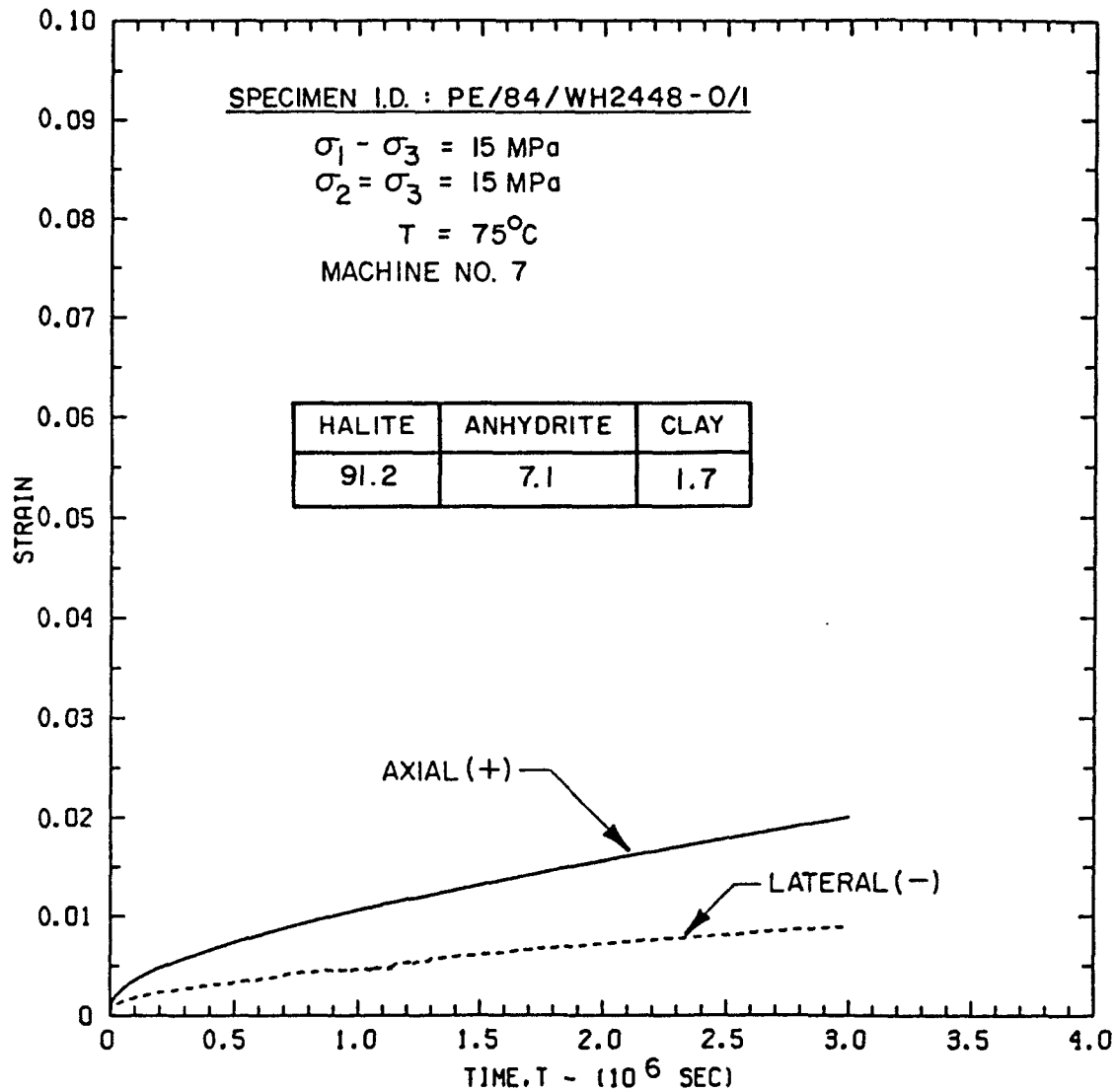

Figure A-5. Measured Axial and Lateral Creep Strain for Palo Duro Salt Specimen PE/84/WH2448-0/1

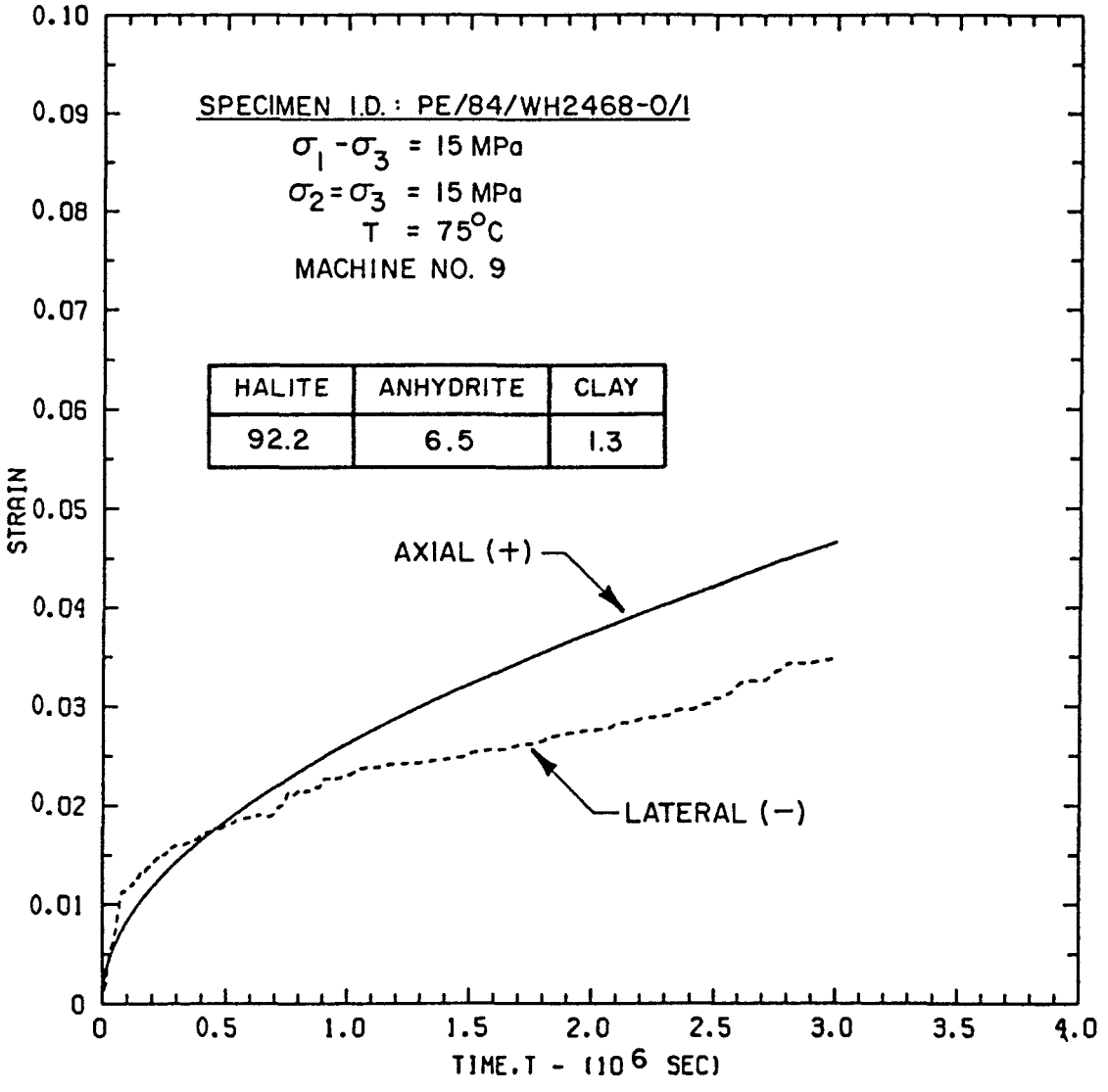

Figure A-6. Measured Axial and Lateral Creep Strain for Palo Duro Salt Specimen PE/84/WH2468-O/1

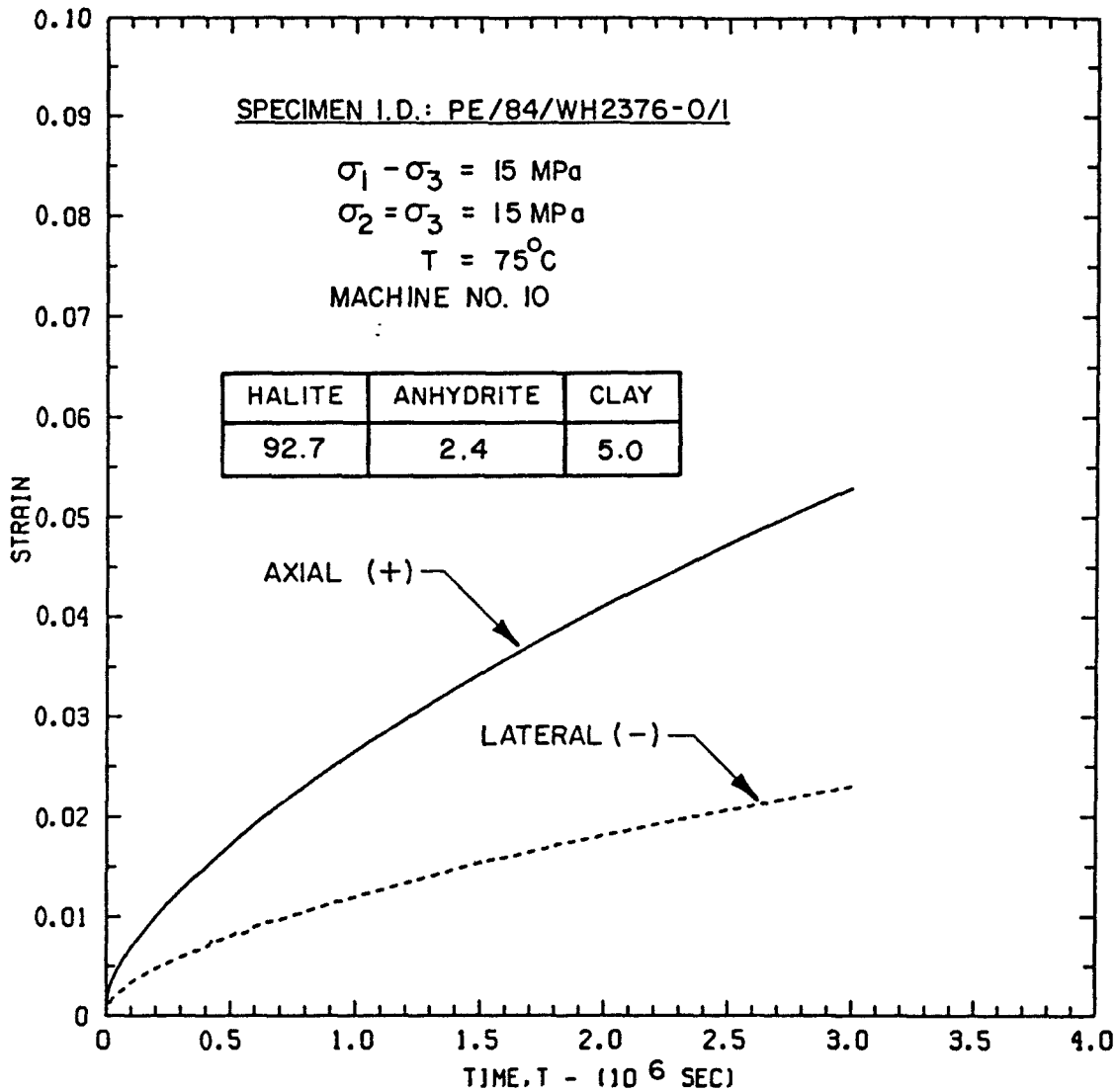

Figure A-7. Measured Axial and Lateral Creep Strain for Palo Duro Salt Specimen PE/84/WH2376-O/1

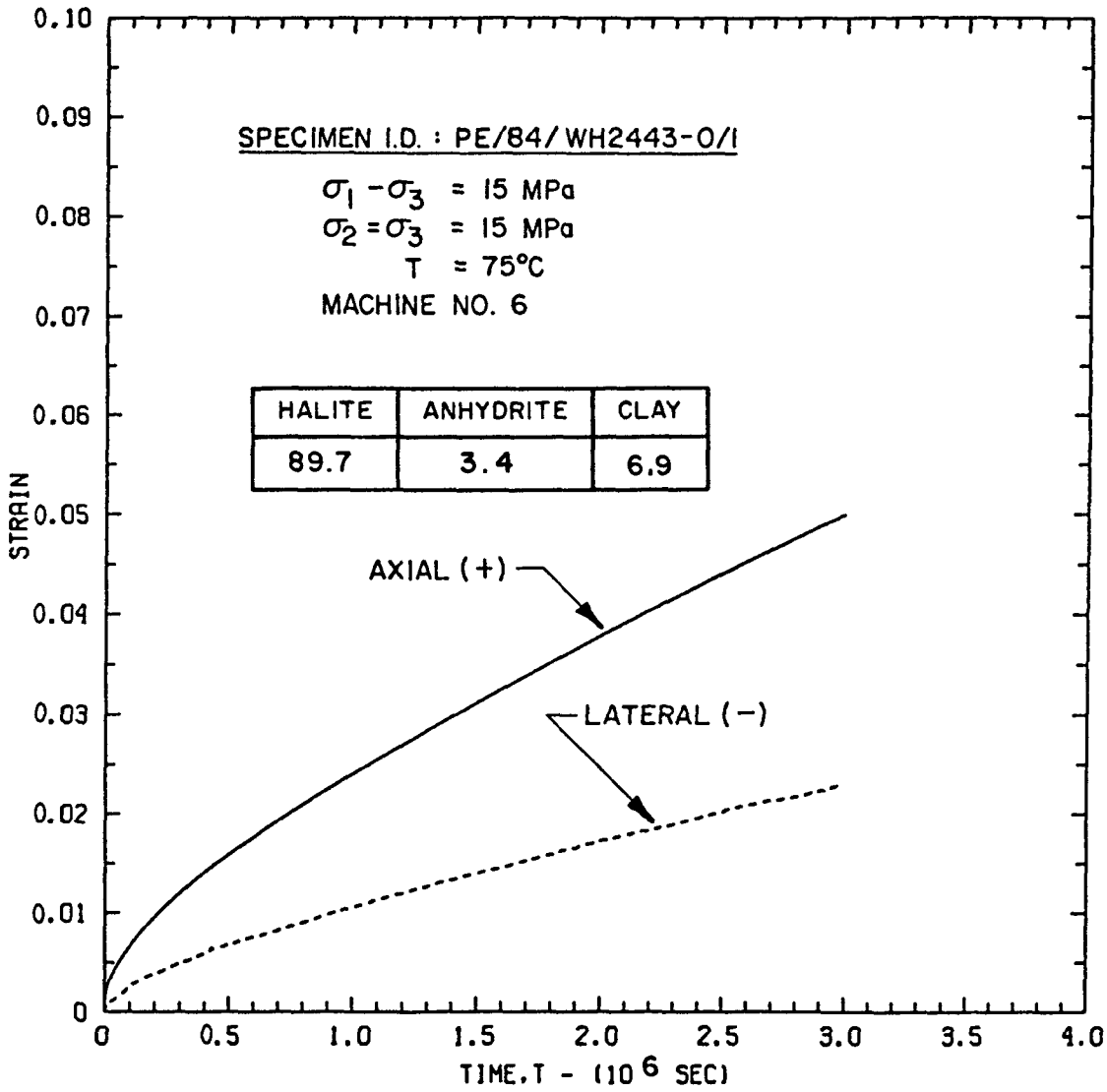

Figure A-8. Measured Axial and Lateral Creep Strain for Palo Duro Salt Specimen PE/84/WH2443-0/1

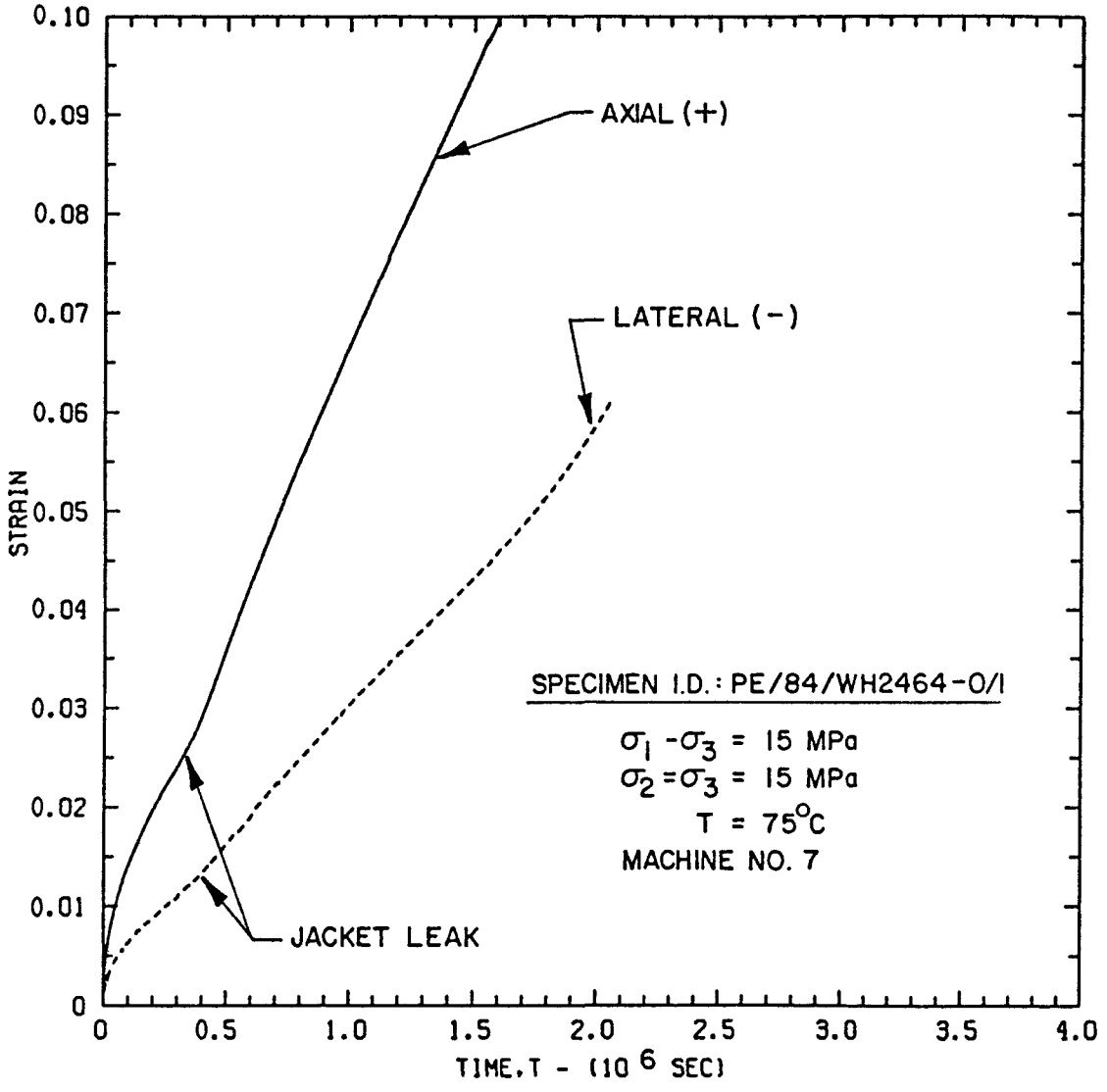

Figure A-9. Measured Axial and Lateral Creep Strain for Palo Duro Salt Specimen PE/84/WH2464-O/1

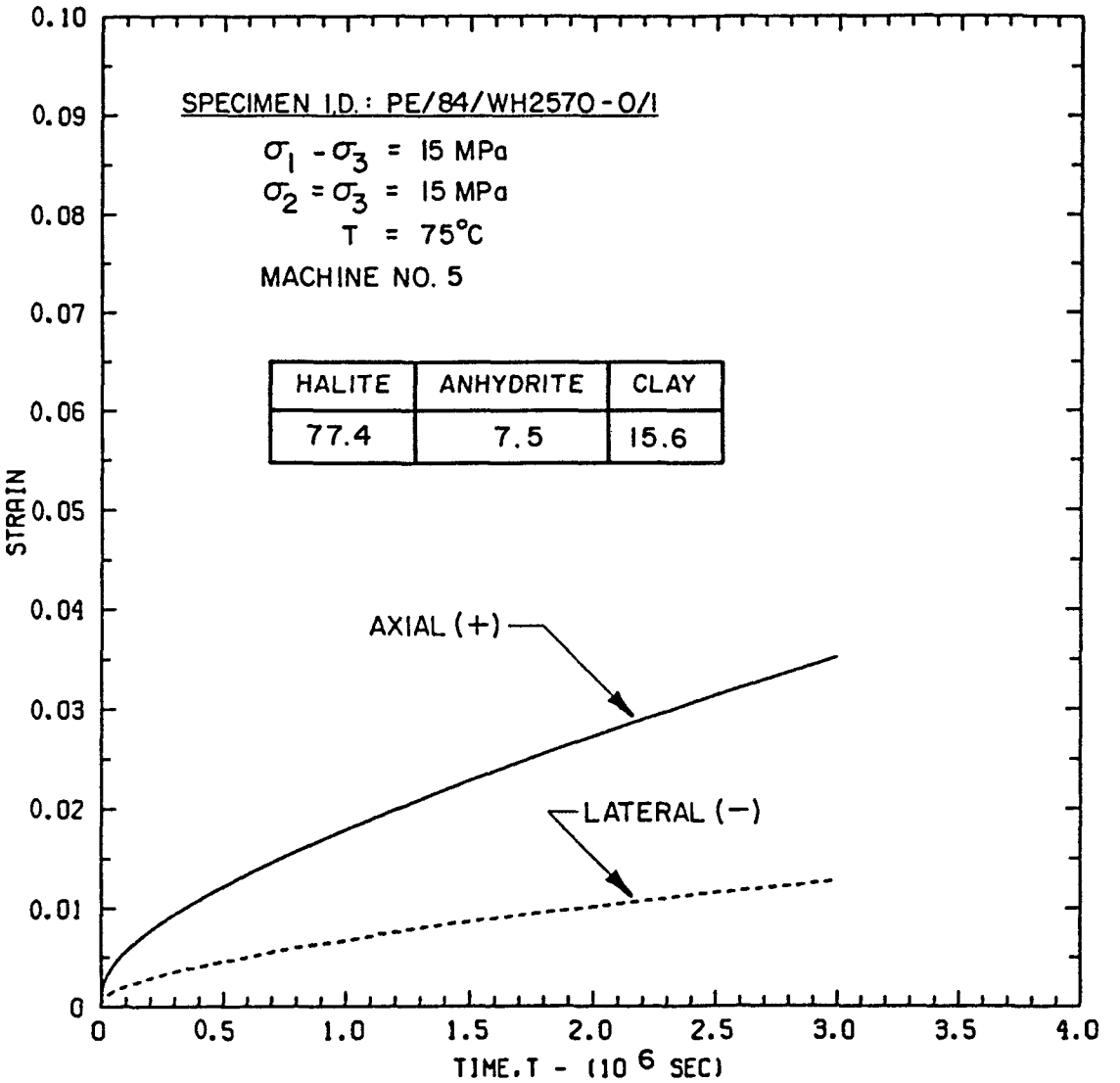

Figure A-10. Measured Axial and Lateral Creep Strain for Palo Duro Salt Specimen PE/84/WH2570-O/1

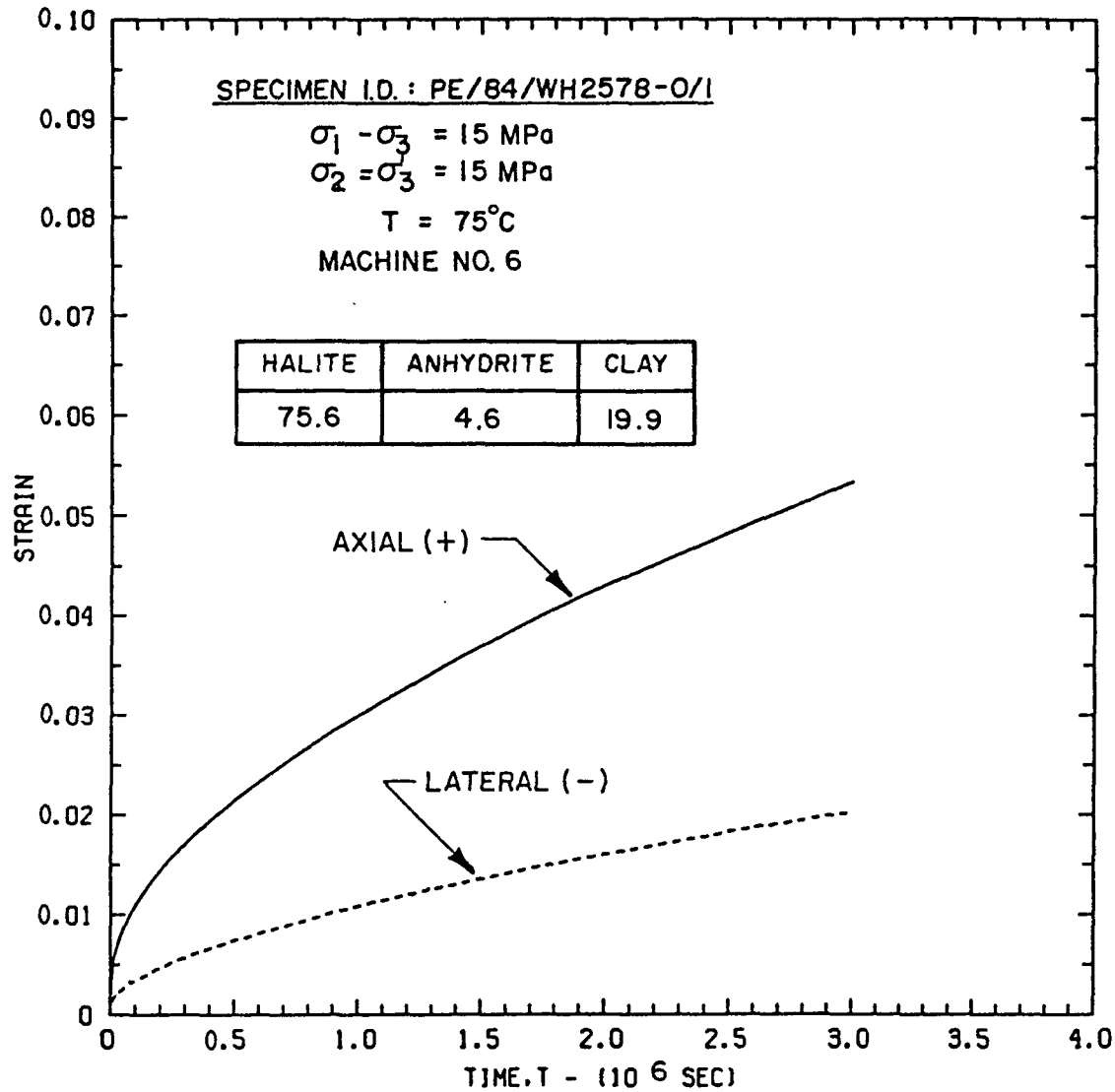

Figure A-11. Measured Axial and Lateral Creep Strain for Palo Duro Salt Specimen PE/84/WH2578-O/1

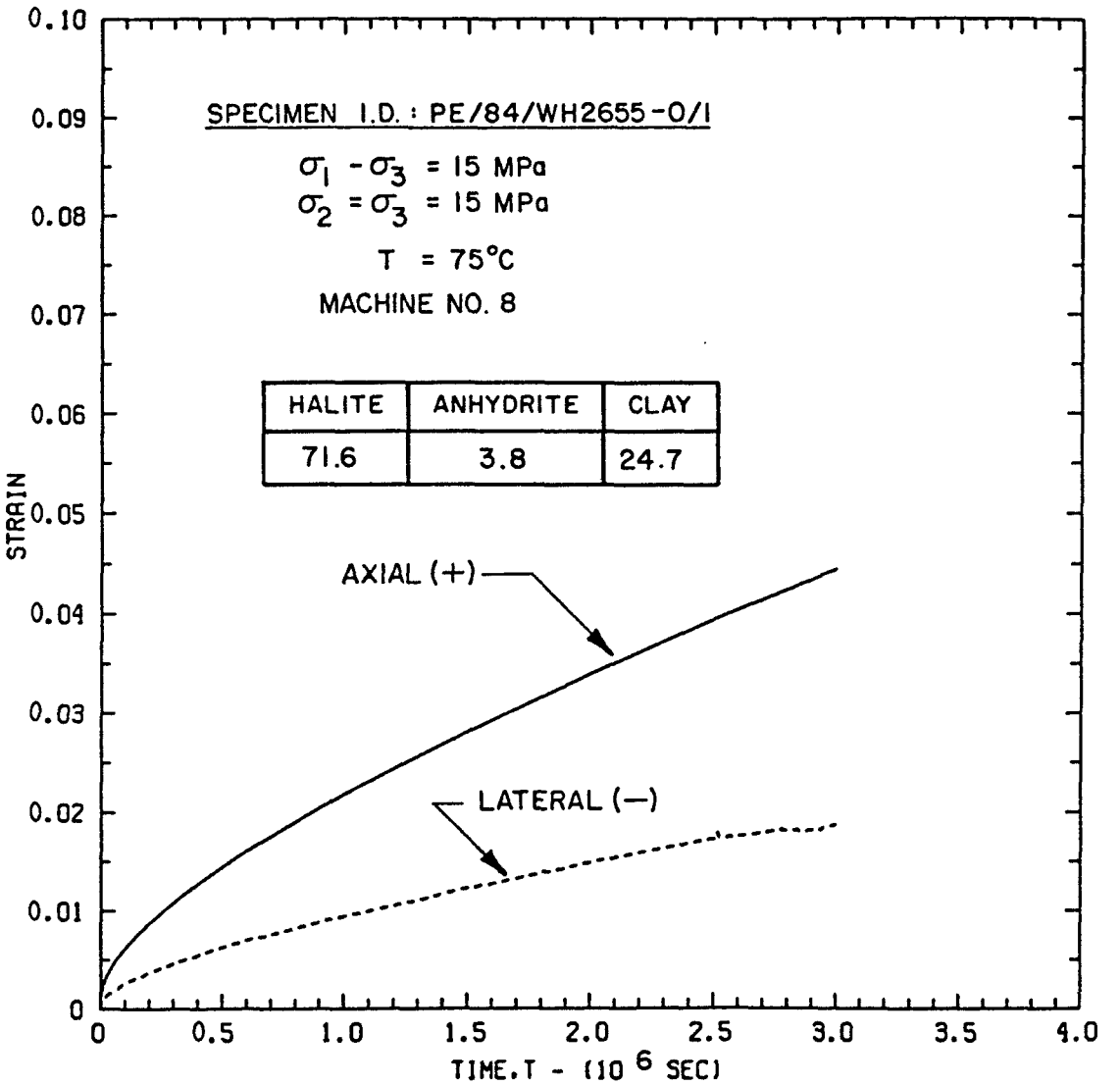

Figure A-12. Measured Axial and Lateral Creep Strain for Palo Duro Salt Specimen PE/84/WH2655-O/1

APPENDIX B

REFERENCE LETTER FOR X-RAY FLUORESCENCE

Missing Page
from
Original Document

July 18, 1984

Battelle
Pacific Northwest Laboratories
P.O. Box 999
Richland, Washington U.S.A. 99352
Telephone (509)
Telex 15-2874

Charles A. Jones
Bendix Field Engineering
P. O. Box 1569
Grand Junction, CO 81501

Dear Charles:

XRF Data on Bedded Salt Cores

In reference to my letter dated February 3, 1984, we received a dozen of 12-inch bedded salt cores from Austin, TX for the continuous XRF analysis. These cores are from Woods-Holtzclaw No. 1 Well. These cores have been analyzed for Cl, Ca, Ti, Fe, Pb, Br, and Sr elements by our continuous XRF scanning device using ^{55}Fe and ^{109}Cd isotopic sources. Each core was scanned at an interval of 1/4 inch per minute for two minutes. The data tables for the seven elements, the individual elemental distance profile and distance profiles of Cl/Br and Ca/Sr ratios of each of the cores are enclosed.

The absolute concentrations of these elements may change somewhat as we still need to correct for matrix effect. However, the relative variations or elemental ratios as a function of distance will remain unchanged. We plan to analyze commercially available anhydride, halite, gypsum, calcium carbonate and dolomite standards to account for matrix effect. Thus, the data presented here is preliminary at this stage.

Certain elements such as Ca and Cl, indicators of gypsum ($CaSO_4$) and halite (NaCl), do show complimentary patterns. The ratios Cl/Br and Ca/Sr ratios do show strong variations with inclusions or changes in lithologies as a function of distance. These variations provide a very useful criteria for further selecting a segment of a core for detailed and additional studies. The continuous scanning XRF device offers a very promising future for core cataloging.

With best regards,

J. C. Laul
Staff Scientist
Radiological Sciences Department

JCL:dlc

Encl. (Not Included in This Report)

cc: N. Hubbard
Stone and Webster

Missing Page
from
Original Document

APPENDIX C

MECHANICAL RESULTS VERSUS IMPURITY CONTENT

Missing Page
from
Original Document

APPENDIX C

LIST OF FIGURES

		Page
C-1.	Steady-State Strain Rate Versus Halite Content	71
C-2.	Steady-State Strain Rate Versus Anydrite Content	72
C-3.	Steady-State Strain Rate Versus Clay Content	73
C-4.	Asymptotic Transient Strain Versus Halite Content	74
C-5.	Asymptotic Transient Strain Versus Anhydrite Content	75
C-6.	Asymptotic Transient Strain Versus Clay Content	76
C-7.	Rate Parameter Versus Halite Content	77
C-8.	Rate Parameter Versus Anhydrite Content	78
C-9.	Rate Parameter Versus Clay Content	79
C-10.	Axial Strain Versus Halite Content	80
C-11.	Axial Strain Versus Anhydrite Content	81
C-12.	Axial Strain Versus Clay Content	82

Missing Page
from
Original Document

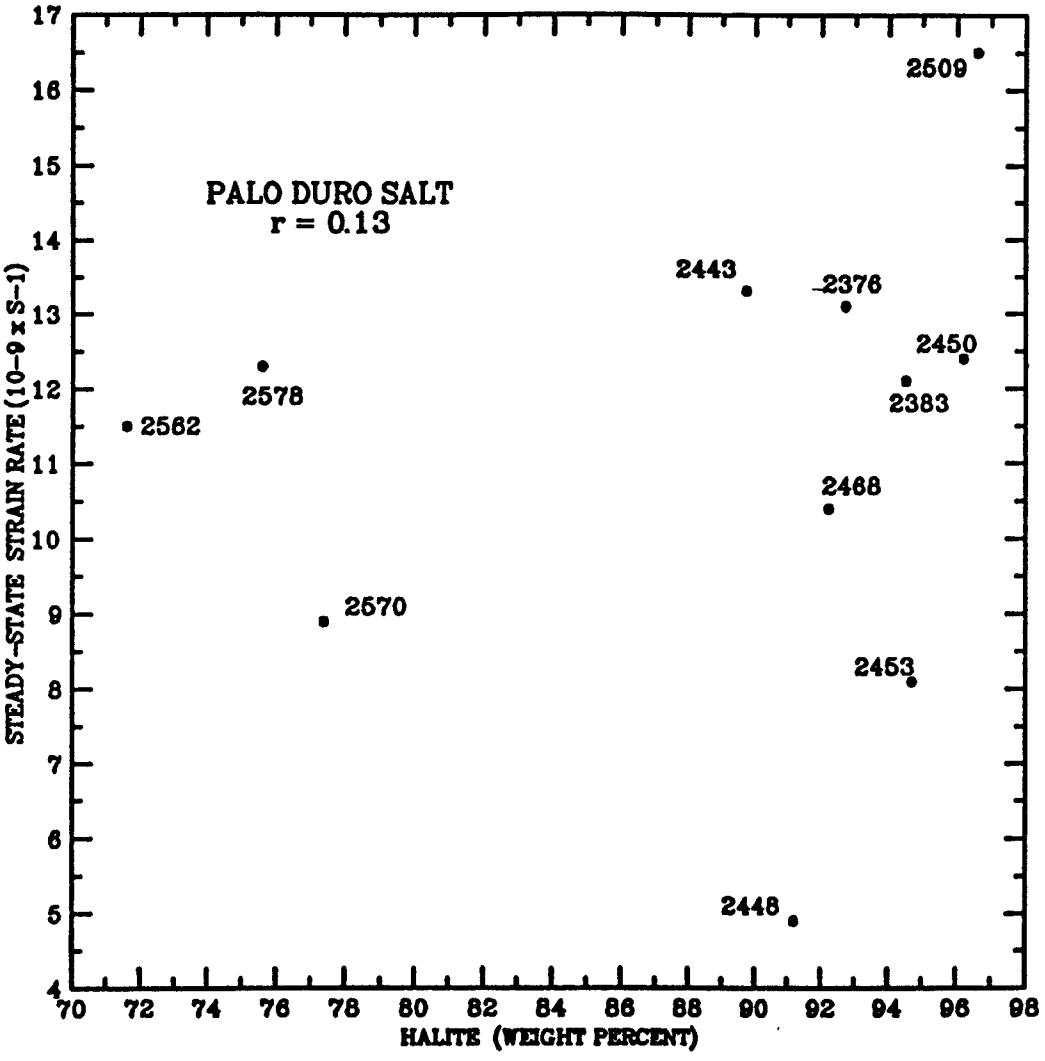

Figure C-1. Steady-State Strain Rate Versus Halite Content

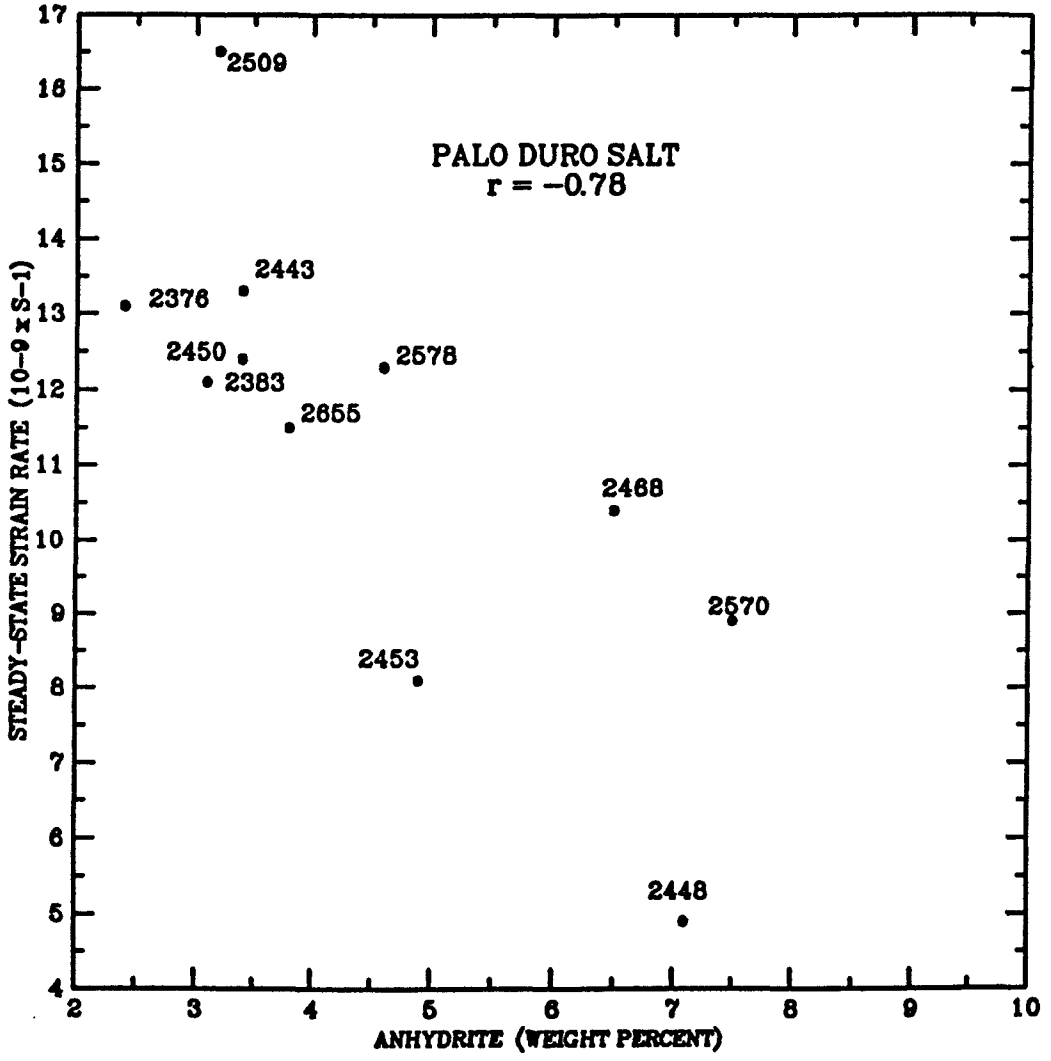

Figure C-2. Steady-State Strain Rate Versus Anhydrite Content

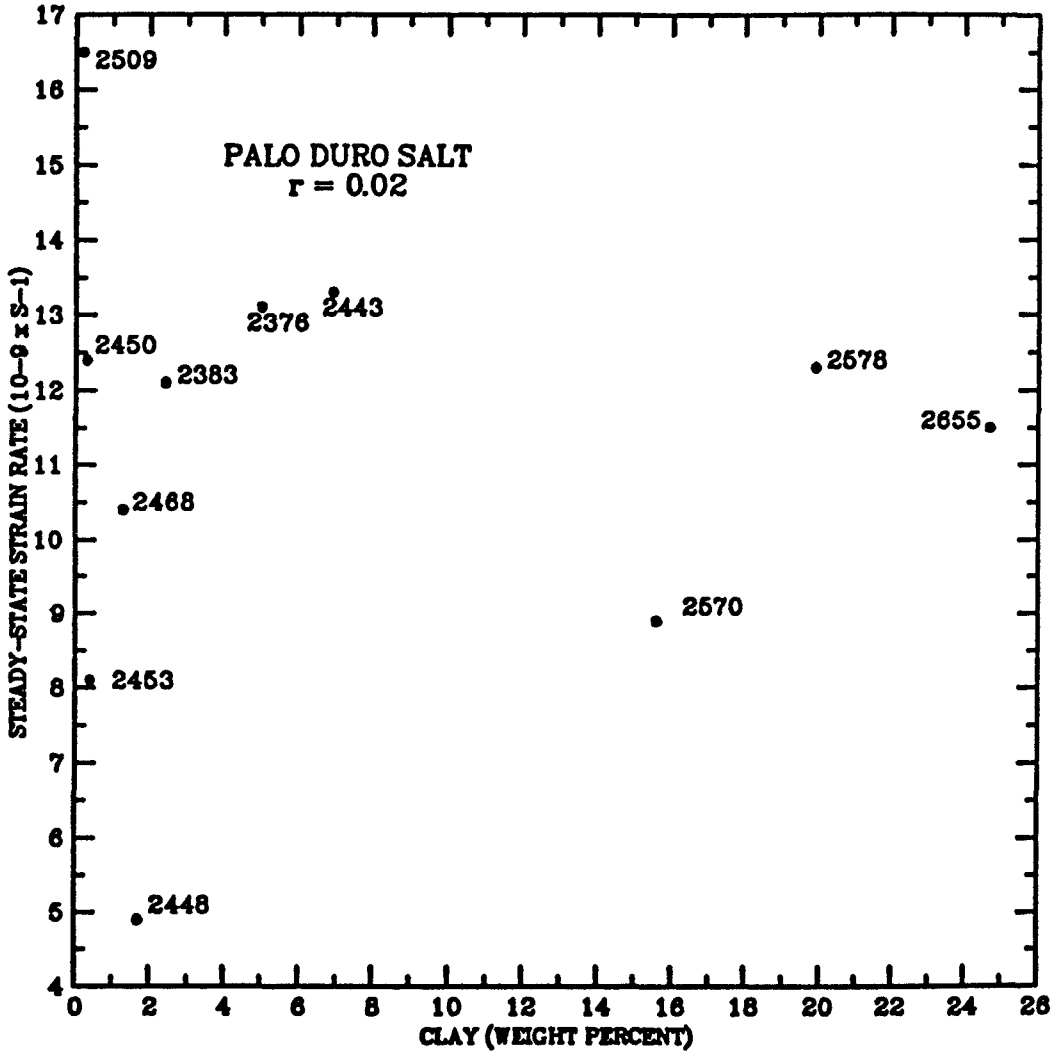

Figure C-3. Steady-State Strain Rate Versus Clay Content

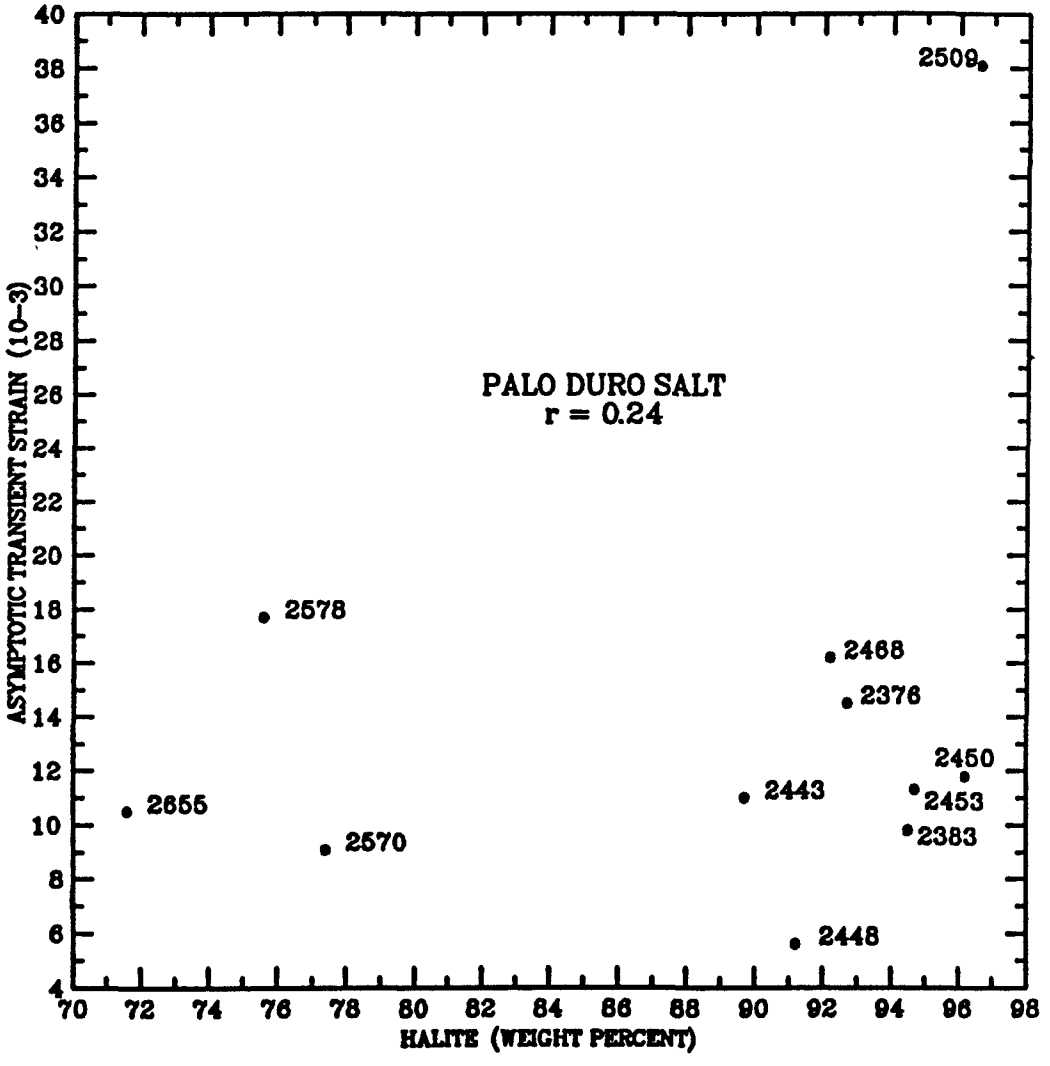

Figure C-4. Asymptotic Transient Strain Versus Halite Content

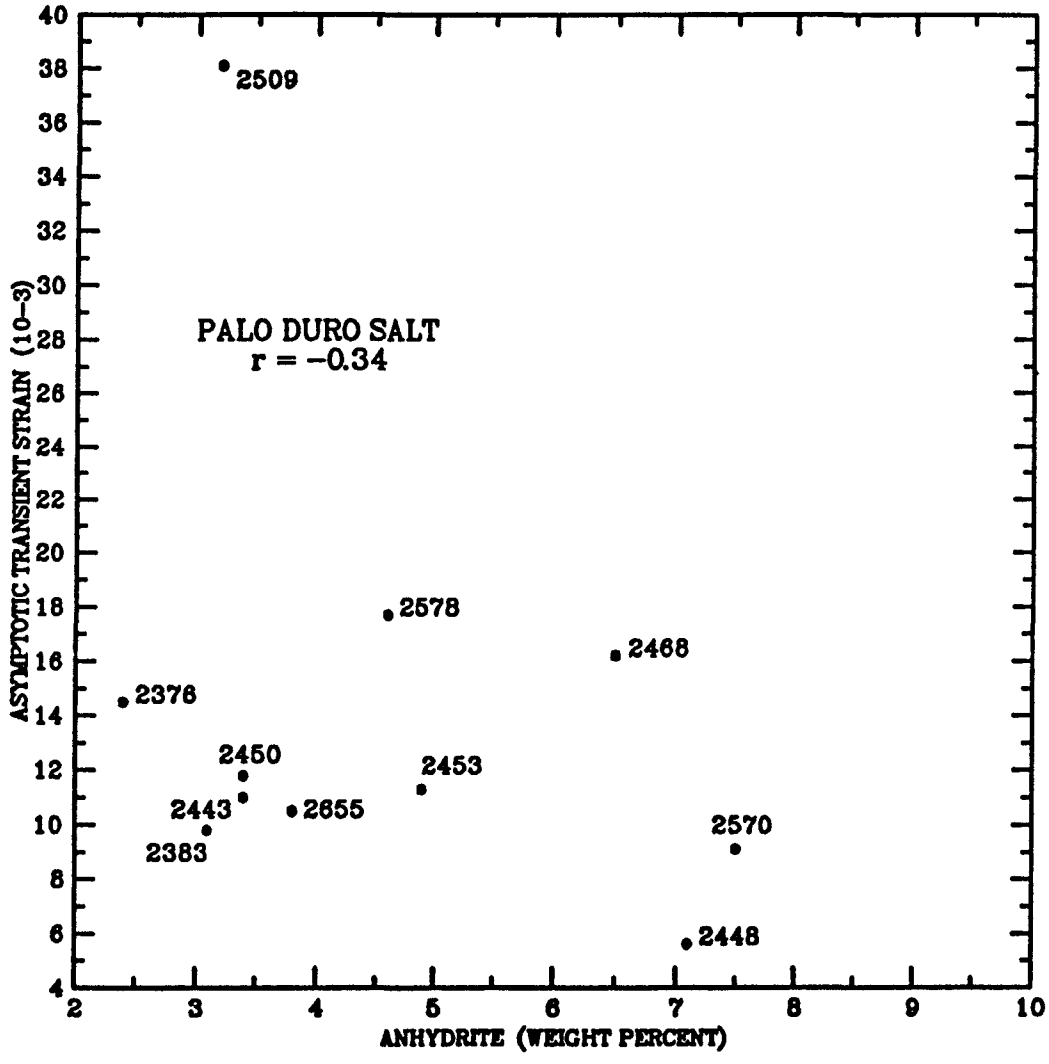

Figure C-5. Asymptotic Transient Strain Versus Anhydrite Content

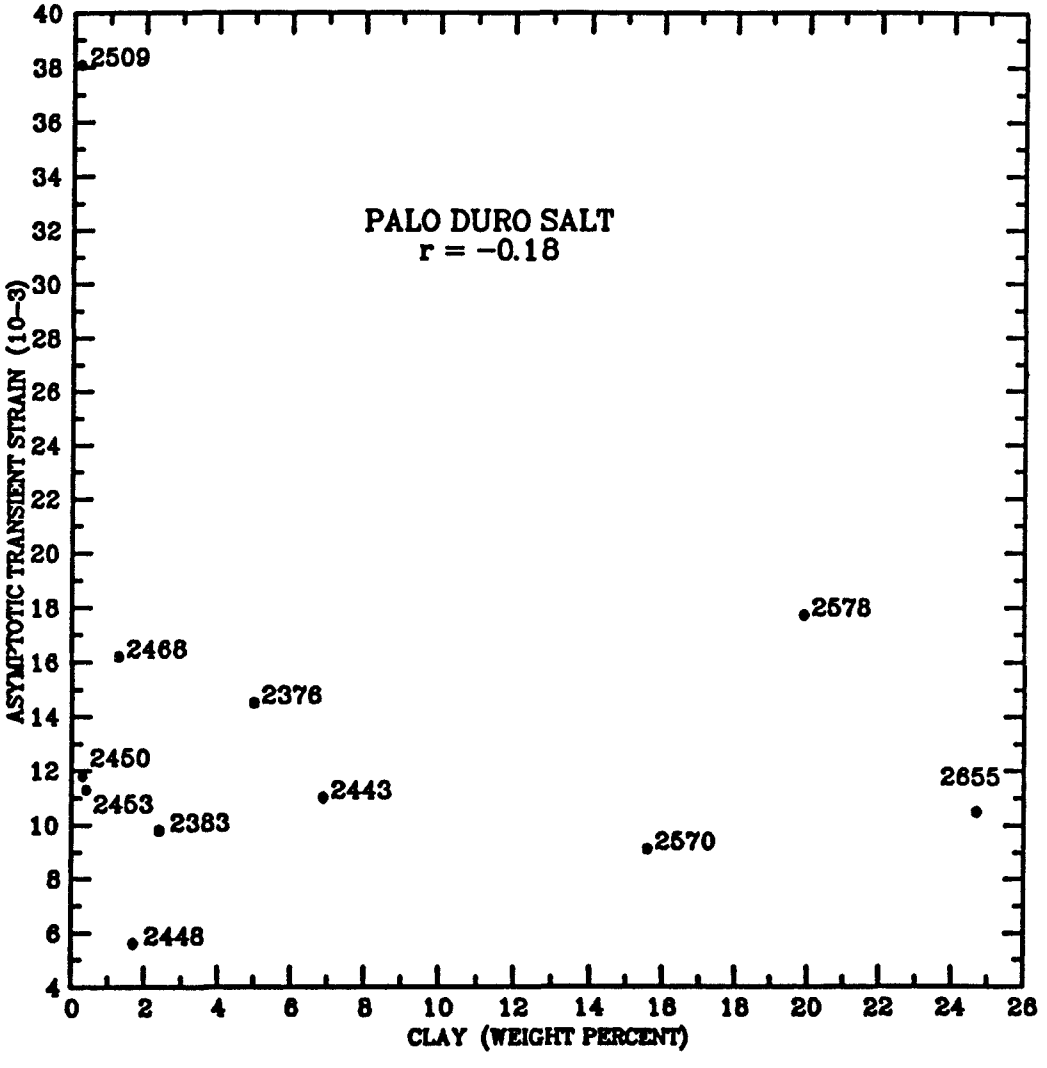

Figure C-6. Asymptotic Transient Strain Versus Clay Content

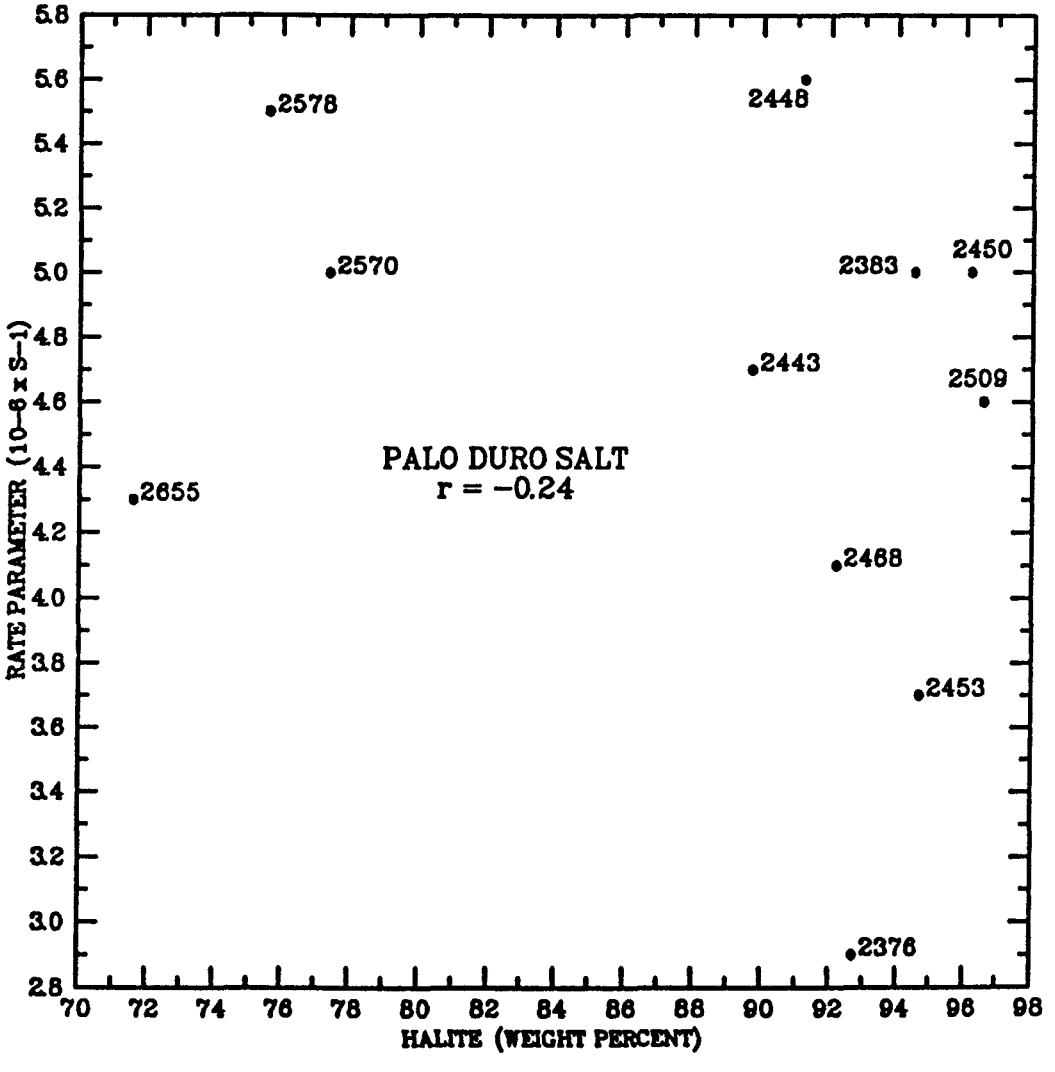

Figure C-7. Rate Parameter Versus Halite Content

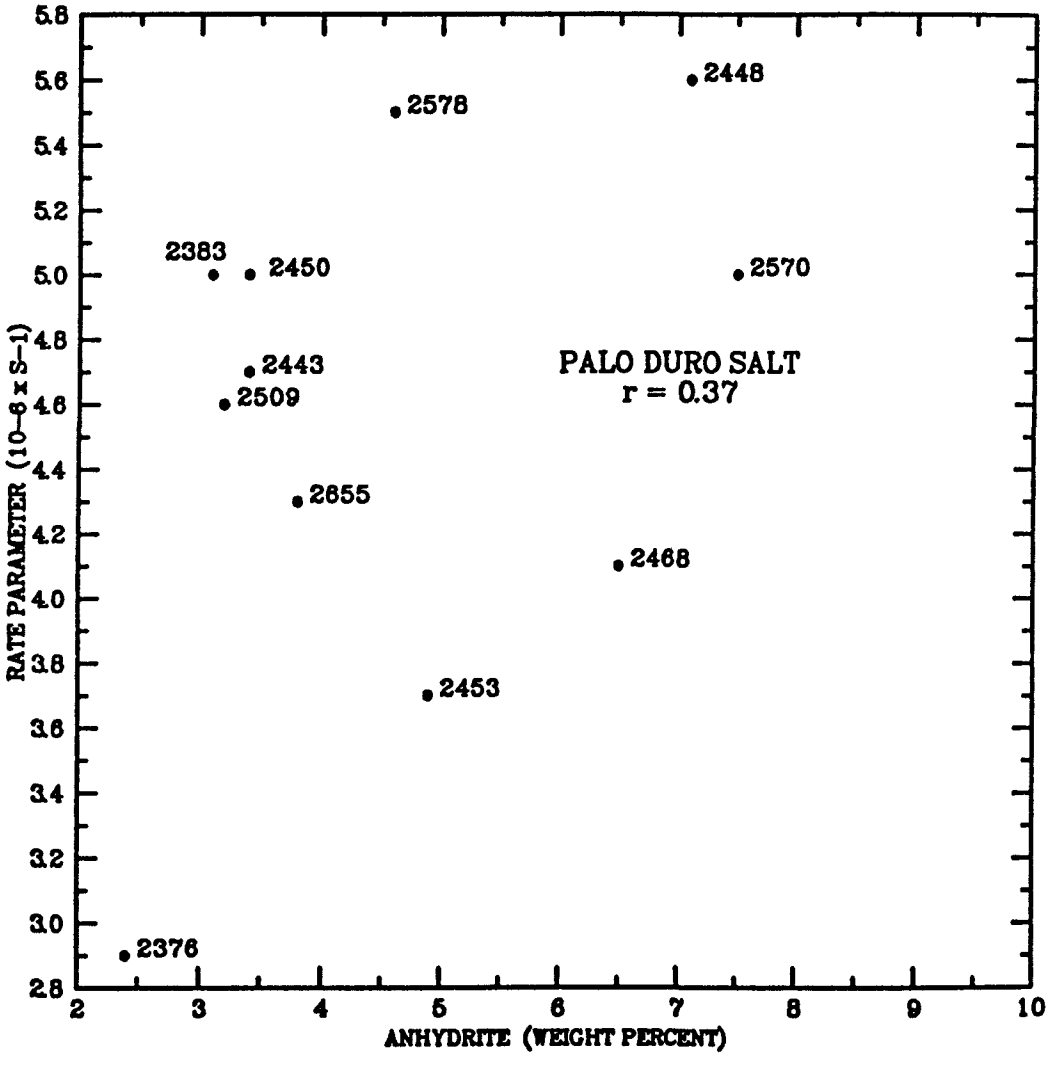

Figure C-8. Rate Parameter Versus Anhydrite Content

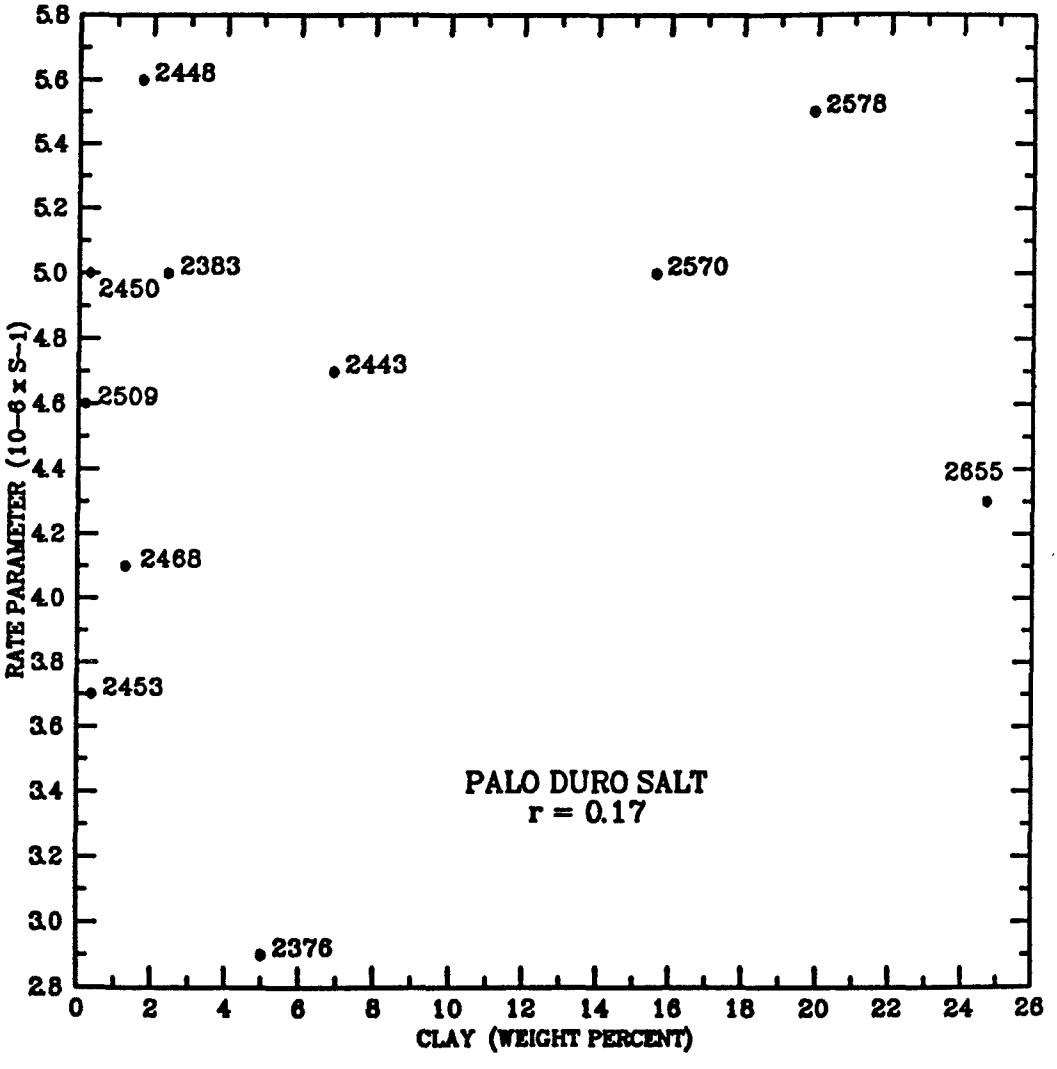

Figure C-9. Rate Parameter Versus Clay Content

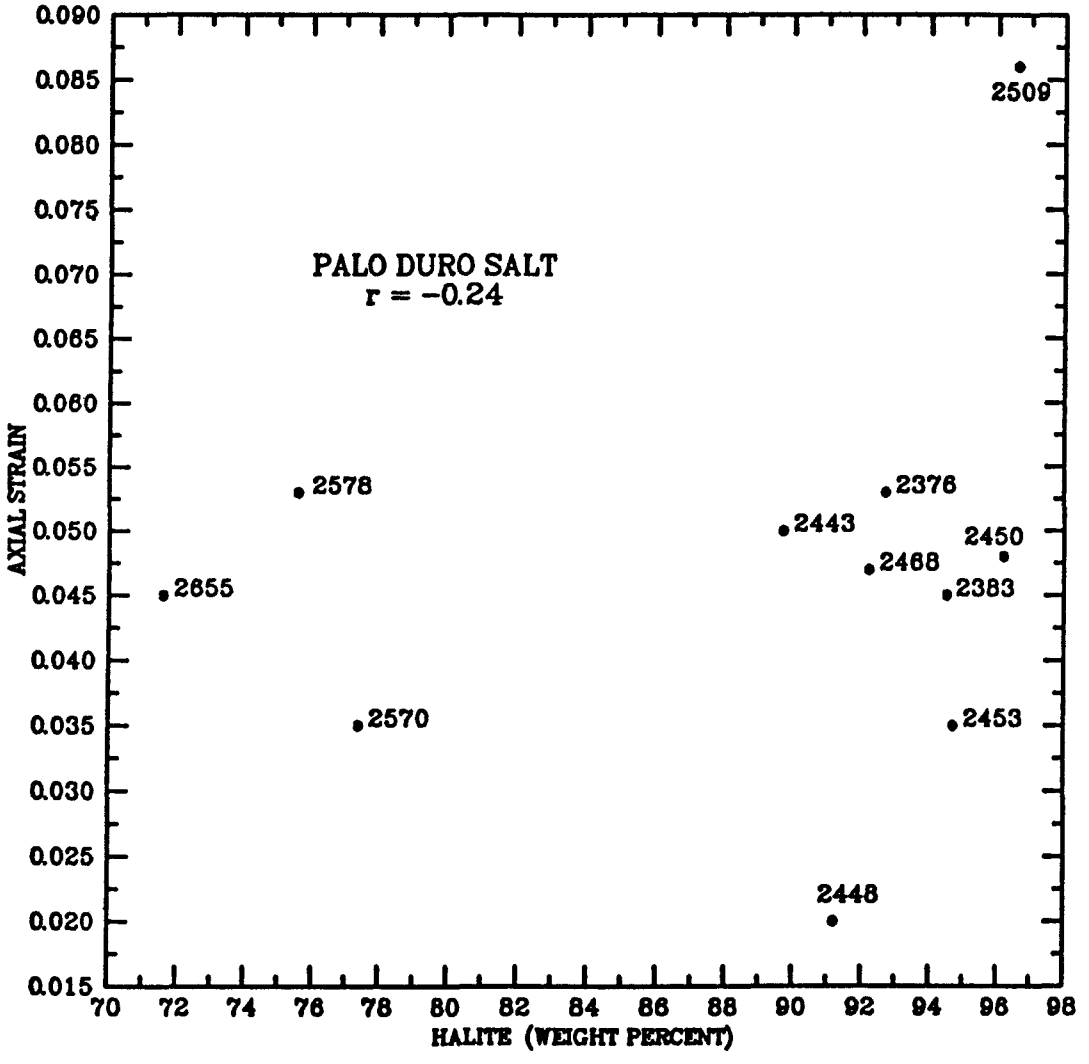

Figure C-10. Axial Strain Versus Halite Content

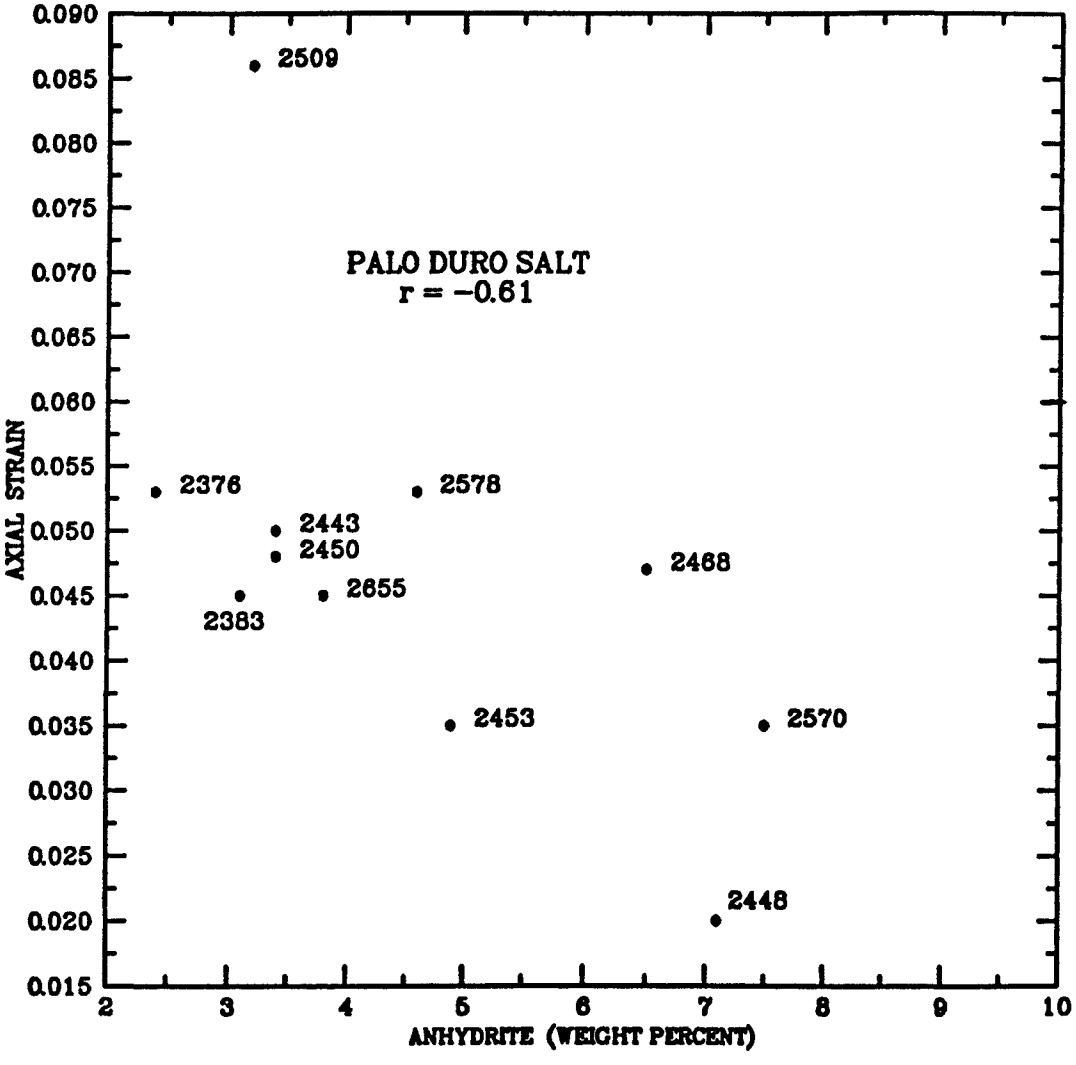

Figure C-11. Axial Strain Versus Anhydrite Content

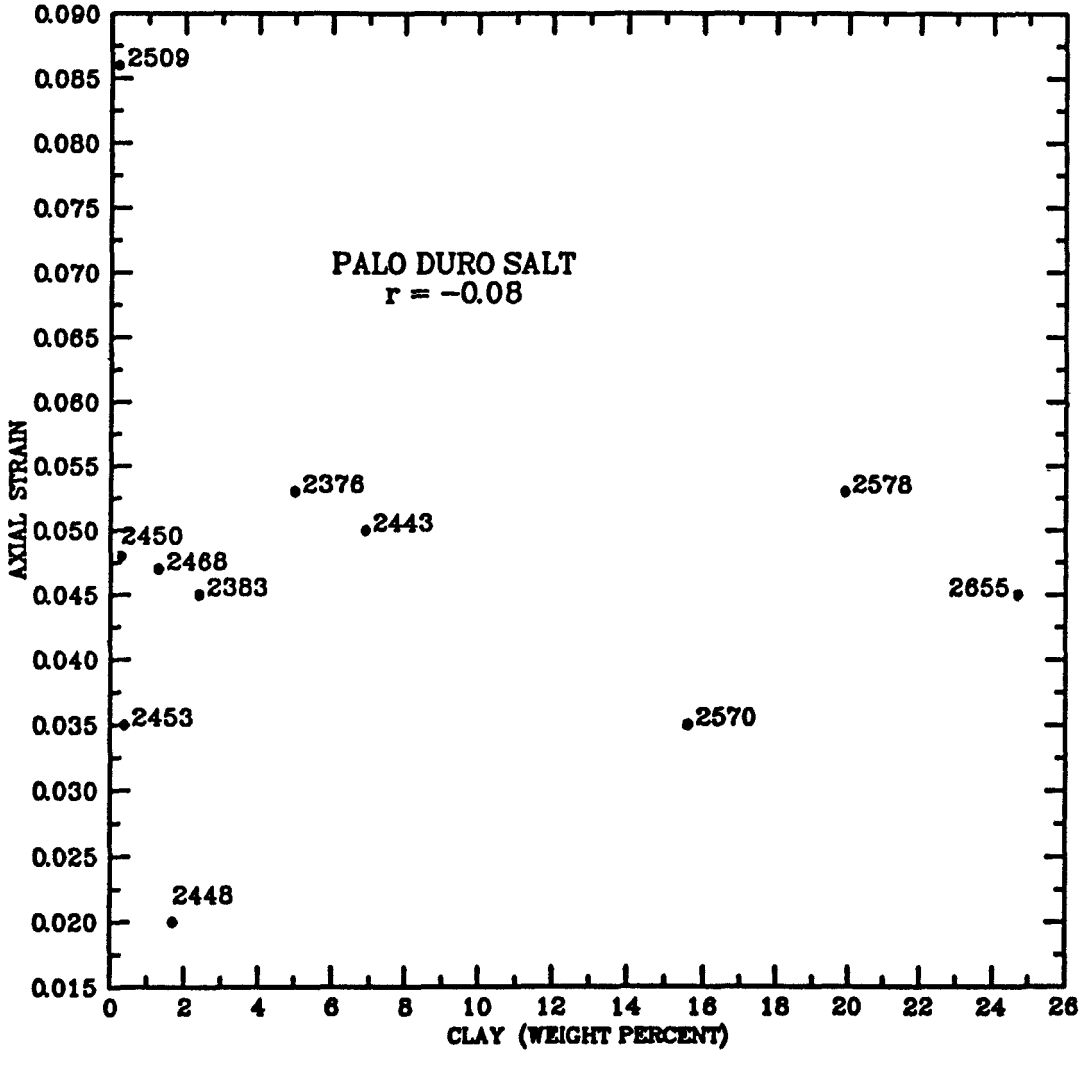

Figure C-12. Axial Strain Versus Clay Content